



1

2 **Rapid assessment of drivers and air quality effects of**
3 **regional daily changes in air pollutant emissions based on**
4 **near-real-time techniques: A case in Jiangsu Province, China**

5

6 Chen Gu¹, Yutong Wang^{1,5}, Yuan Ji¹, Lei Zhang^{1,2}, Shuanzhu Sun³, Yuandong Bian¹,
7 Zimeng Zhang¹, Jiewen Zhu³, Wenxin Zhao¹, Sheng Zhong⁴, Yu Zhao^{1,2*}

8

9 ¹ State Key Laboratory of Water Pollution Control and Green Resource Recycling and
10 School of Environment, Nanjing University, 163 Xianlin Rd., Nanjing, Jiangsu
11 210023, China

12 ² Collaborative Innovation Center of Atmospheric Environment and Equipment
13 Technology, CICAET, Nanjing, Jiangsu 210044, China

14 ³ Jiangsu Frontier Electric Power Technology Co., Ltd., 58 Suyuan Ave., Nanjing,
15 Jiangsu 211102, China

16 ⁴ Jiangsu Provincial Environmental Monitoring Center, 100 Zhonghe Rd., Nanjing
17 210013, China

18 ⁵ Key Laboratory of Formation and Prevention of Urban Air Pollution Complex,
19 Ministry of Ecology and Environment, Shanghai Academy of Environment Sciences,
20 Shanghai 200233, P. R. China

21

22 *Corresponding author: Yu Zhao

23 Phone: 86-25-89680650; Email: yuzhao@nju.edu.cn

24

25

26



27 ABSTRACT

28 Fast and timely estimation of changing air pollutant emissions is critical for
29 understanding the complex sources of air pollution and supporting air quality
30 improvement, while current regional emission inventory was commonly reported with
31 time lag or coarse temporal resolution. Here we developed a near-real-time approach
32 that calculates the daily emissions of anthropogenic air pollutants, and applied this
33 approach for Jiangsu province, a typical developed region in eastern China. We
34 estimated that the annual total anthropogenic emissions of SO_2 , NO_x , primary fine
35 particles ($\text{PM}_{2.5}$), non-methane volatile organic compounds (NMVOCs), and NH_3
36 were 246, 727, 298, 1186, and 377 Gg, respectively, for Jiangsu in 2022. Compared to
37 the national emission inventory, application of the provincial-level daily emission
38 estimates provided better model performance of $\text{PM}_{2.5}$ and ozone (O_3) simulation for
39 all the involved months. The NO_x , SO_2 , $\text{PM}_{2.5}$, and NMVOCs emissions in Jiangsu
40 during April-May 2022 (the period of COVID-19 lockdown in Shanghai) were
41 respectively 8%, 6%, 6%, and 10% smaller than those in the same period of 2023.
42 Transportation and Industry respectively contributed 89% of NO_x emission reduction
43 and 93% NMVOCs reduction. Combining with machine learning algorithms,
44 moreover, we revealed that the changing agricultural NH_3 emissions dominated the
45 variability of daily $\text{PM}_{2.5}$ concentration, and that off-road transportation contributed
46 substantially to variabilities of both $\text{PM}_{2.5}$ and O_3 levels. The study proved advantages
47 of incorporation of near-real-time data and machine learning techniques on tracking
48 the fast-changing emissions and detecting the sources of varying air quality.

49



50 1. Introduction

51 Emissions of air pollutants from anthropogenic activity including traffic, industrial
52 plants, and residential and commercial fuel consumption are the main cause of
53 worsened air quality, especially in economically developed regions with dense
54 populations (Sokhi et al., 2022; Zheng et al., 2018). Emission inventory, which
55 contains complete information on magnitude, spatial pattern, and temporal change of
56 air pollutant emissions by sector, is essential for identifying the sources of air
57 pollution and effectiveness of emission controls on air quality through numerical
58 modeling (Zhao et al., 2013; Zhang et al., 2019). Traditionally, “bottom-up”
59 methodology (i.e., the emissions were calculated for the finest source categories and
60 then aggregated to bigger categories) provides robust time series of emission
61 estimates based on national statistics (An et al., 2021; Crippa et al., 2020; Kurokawa
62 et al., 2020). However, these emission estimates were usually reported with a time lag
63 of at least 3-5 years. The delay reflected the time needed to finalize accurate national
64 statistics (e.g., official energy consumption by fuel type) and that needed to collect
65 and process them for compiling emission inventories (Guevara et al., 2023). As a
66 result, in addition to the inherent uncertainties in emission inventories, this delay can
67 introduce extra uncertainty when these inventories are employed in air quality
68 modeling, as they may miss current emission characteristics (Tong et al., 2012). Such
69 limitation can be greatly exacerbated for periods with big and unexpected emission
70 fluctuations, resulting from temporary actions for major events or public health
71 incidents (Huang et al., 2021; Wang et al., 2025).

72 To better track the changing emissions for specific events or incidents (e.g.,
73 COVID-19 pandemic), researchers have developed alternative methods to obtain the
74 near-real-time emission estimates (Gaubert et al., 2021; Schneider et al., 2022). The
75 objective of these efforts is to understand the driving factors of the changing
76 emissions and their impact on air quality. Real-time activity information with high
77 temporal resolution started to be incorporated in the emission estimation, such as the



78 electricity load and generation data by national transmission system operators, the
79 real-time vehicle flows monitored from navigation applications, and the real-time ship
80 navigational information from automatic identification system (AIS) (Liu et al., 2020a;
81 Liu et al., 2020b; Zheng et al., 2021; Huang et al., 2021; Harkins et al., 2021; Guevara
82 et al., 2021). Although limited availability and huge capacity of these data hinder their
83 full use in emission inventory development, there is a big potential in expanding the
84 data source to improve the capability of capturing the fast-changing emissions.

85 Currently, studies have been conducted for carbon dioxides (CO₂) emissions and
86 near-real-time data platforms and products have been developed, particularly for
87 well-identified stationary sources such as fossil fuel combustion plants (BEIS, 2022;
88 CBS, 2024; CITEPA, 2024; Carbon Monitor, 2024). Comparatively, achieving
89 near-real-time estimates is more challenging for air pollutants due to the large
90 complexity and variability of their emission processes. A great variety of air pollutants
91 come from a wide range of sources, containing fuel combustion, industrial processes,
92 on-road and off-road traffic, solvent evaporation, and agricultural activities (Xu et al.,
93 2023; Zheng et al., 2020). The emissions can be greatly influenced by many factors
94 and change a lot. Those factors include the human behavior patterns, operating
95 conditions of plants, improved use of manufacturing and pollution control
96 technologies, and/or meteorological conditions (Liu et al., 2024; Lei et al., 2023;
97 Geng et al., 2024). Given the strong chemical reactivity and short atmospheric
98 lifetime of many air pollutants, there exist complicated relationships between
99 emissions and air quality, emphasizing the importance of tracking the fast-changing
100 emissions (Liu et al., 2020; Zhao et al., 2020a). Therefore, efforts are still in great
101 need to develop effective approach for estimating the near-real-time emissions.

102 For the past years, China has substantially enhanced emission control for industrial
103 (e.g., “ultra-low” emission retrofit for selected non-electrical industries) and
104 residential sources (e.g., promotion of advanced stoves and clean coals during heating
105 seasons). Those measures have clearly reduced emissions of many air pollutants,
106 resulting in a 17.2 µg/m³ decline of fine particle (PM_{2.5}) concentration between 2015



107 and 2020 over the country (Geng et al., 2024). In contrast, the emissions of NO_x and
108 PM_{2.5} from passenger transportation respectively grew by 178% and 152% from 2019
109 to 2022 (Zhang et al., 2023), and the maximum daily 8h mean ozone (MDA8 O₃)
110 concentrations increased 5.8% from 2021 to 2022 for the country (MEE, 2023). The
111 diverse changes in emissions and air quality highlight the necessity to quickly and
112 accurately reveal the drivers of changes in air pollutant emissions and their impact on
113 ambient air quality (Gu et al., 2023). This is particularly important for periods with
114 severe air pollution episodes and unexpected incidents that substantially changed
115 human activities like COVID-19 lockdown, as timely temporary actions to address
116 pollution might be urgently required.

117 Province serves as a crucial role in air quality management in China. Due to
118 difference in economic and energy structure and atmospheric conditions, local
119 governments often implement diverse strategies and actions to reduce regional air
120 pollution. This results in large variability in both emission and air quality changes
121 across different regions. (Liu et al., 2022; Wang et al., 2021). Studies relying on
122 national emission data offer limited guidance in developing emission control
123 measures and assessing their effectiveness in air quality improvement (An et al.,
124 2021). Jiangsu Province, located in the Yangtze River Delta (YRD) in eastern China,
125 is one of most economically developed regions across the country (Supplementary
126 Figure S1). It accounted for 10.2% of the gross domestic product (GDP) in mainland
127 China (ranking the second place in the country), and 8.1%, 12.4% and 11.6% of coal
128 consumption, cement and crude steel production in 2022, respectively (NBS, 2023).
129 Following the implementation of air pollution prevention measures, the PM_{2.5}
130 pollution in Jiangsu has significantly decreased since 2015. However, the
131 development of the petrochemical industry and transportation has led to rapid changes
132 in emissions, making Jiangsu as the province with the highest and fastest growing O₃
133 concentration in YRD in recent years (Zhou et al., 2017; Wang et al., 2022).

134 In this study, therefore, we selected Jiangsu as an example to demonstrate the
135 development of near-real-time emission inventory and its application on rapid



136 assessment of air quality. Based on our previous work that incorporated the best
137 available facility-level information to develop a comprehensive provincial emission
138 inventory (Gu et al., 2023), here we constructed an approach driven by real-time
139 activity data from multiple sources. The pollutants include SO_2 , NO_x , primary $\text{PM}_{2.5}$,
140 NH_3 , and non-methane volatile organic compounds (NMVOCs). We then applied the
141 method to obtain the near-real-time emission estimates for 2022-2023, and assessed
142 the driving factors of the short-term emission change during the COVID-19 lockdown
143 period. Finally, we used an Extreme Gradient Boosting (XGBoost) algorithm to
144 explore the relationship between the variability of daily $\text{PM}_{2.5}$ and O_3 concentrations
145 and their precursor emissions for 2022. The study provides insights for timely design
146 and implementation of air pollution control actions, and can be used for reference for
147 other developed and polluted regions in China and worldwide.

148 **2. Methodology and data**

149 **2.1 Framework of near-real-time emission estimation**

150 Figure 1 shows the methodological framework. In our previous study (Gu et al., 2023),
151 we collected, examined, and integrated most available information on emission
152 sources to enhance the completeness and reliability of the provincial emission
153 inventory. All the information, including raw material and energy consumption,
154 product output, and manufacturing and emission control technologies, played an
155 important role in the estimation of near real-time emissions. The specific methods by
156 sector are described in Section 2.2. Furthermore, we improved the spatial distribution
157 of air pollutant emissions. Point sources of power and industrial enterprises were
158 allocated based on their precise latitudes and longitudes. We further utilized Point of
159 Interest (POI) data from Gaode Map (<https://lbs.amap.com/>, last visited on October
160 2025) to obtain the real-time changes on road and waterway networks, land use, and
161 building footprints. The information is updated every 2-3 months. The use of POI data
162 significantly reduced the error of spatial allocation of emissions that may result from
163 the delayed and indirect information on the “surrogate” parameters (Wang et al.,



164 2017).

165 **2.2 Near-real-time daily emission estimation by sector**

166 This section describes the methods for estimating near-real-time daily emissions for
167 2022 and 2023. Six major sectors were included (Power, Industrial plant, Vehicles
168 (On-road transportation), Off-road machinery, Residential, and Agriculture), covering
169 most anthropogenic activities. Road and construction site dusts were not contained.

170 **Power plant** Previously we developed a method of applying online measurement data
171 from the continuous emission monitoring systems (CEMS,
172 <http://218.94.78.61:8080/newPub/web/home.htm>, last visited on October 2025) for
173 emission estimation at the unit/plant level (Zhang et al., 2019). With this basis, we
174 have improved the emission estimation method to enable the stable and continuous
175 acquisition of near-real-time emission data lagged by one month. For the small
176 number of power-generating units without CEMS data, we assumed that their
177 pollutant concentrations in the flue gas were at the average level of units with similar
178 installed capacity (Tang et al., 2019). The emissions were calculated based on the
179 mean hourly flue gas concentration of air pollutant obtained from CEMS and the
180 theoretical flue gas volume of each unit/plant:

$$181 \quad E_{i,j,day} = C_{i,j,month} \times AL_{j,month} \times V_{j,m}^0 \times P_{i,j,m,day} \quad (1)$$

$$182 \quad AL_j = F_m / R_m \quad (2)$$

183 where E is the emission of air pollutant; i, j and m indicate the specific pollutant
184 species, individual power plant or unit, and fuel type, respectively; C is the monthly
185 average concentration in the flue gas; AL is the activity level (here monthly coal
186 consumption); F is the monthly electricity generation for various fuels, as reported by
187 NBS (2023); R is the fuel consumption rate for power generation, taken from Tong et
188 al. (2021), V^0 is the theoretical volume of flue gas produced per unit of fuel
189 consumption (Zhao et al., 2010); P is the temporal profile of emissions (the daily to
190 monthly emission ratio), based on the hourly pollutant concentrations and volume of
191 flue gas for the month and specific day.



192 **Industrial plant** With its gradually expanding penetration, CEMS has become able to
193 support near-real-time emission estimation for industrial plants (Tang et al., 2022; Bo
194 et al., 2021). Given its varying coverage across sectors, we have developed a method
195 that can stably estimate the near-real-time emissions at the plant level with a lag of
196 one month. This method classifies industrial plants into three categories based on their
197 CEMS coverage, as described below.

198 (1) Industrial plants with CEMS information. The method is similar to power plants:

$$199 \quad E_{i,j,day} = C_{i,j,month} \times AL_{j,month} \times V_{i,j,k}^0 \times P_{i,j,m,day} \quad (3)$$

200 where k denotes the industrial sector; AL is the activity level (here represents monthly
201 product output) as reported by NBS (2023), and V^0 is the theoretical volume of flue
202 gas produced per unit of product output, which can be found in the technical
203 specifications for the application of emission permits (MEE, 2021).

204 (2) Industrial plants without CEMS while it was equipped at some plants within the
205 same sector. Sector-level emission factors (emissions per unit of activity level, EF)
206 were calculated using CEMS data from other plants. Monthly emissions were
207 estimated based on the sector-level EF and monthly product output from official
208 environmental statistics. The near-real-time daily emissions were then generated
209 according to the temporal profile of emissions (P) obtained from CEMS installed in
210 other available plants in the sector.

$$211 \quad E_{i,j,day} = AL_{j,month} \times EF_{i,k} \times P_{i,j,m,day} \quad (4)$$

$$212 \quad EF_{i,k} = E_{i,k,month} / AL_{k,month} \quad (5)$$

213 where $EF_{i,k}$ is the sector-average emission factor for plants with CEMS for sector k ,
214 $E_{i,k}$ and AL_k are the total emissions from industrial plants with CEMS and their
215 product output, respectively.

216 (3) Industrial sectors without CEMS data. Emissions were principally calculated
217 based on activity level and emission factor. The activity data were derived based on
218 monthly official statistics reported by NBS (2023). In addition, we analyzed the
219 historical emission source data to trace the evolution of manufacturing and emission
220 control technologies for various sectors, and the emission factors could be calculated



221 for near-real-time emission estimations:

222
$$E_{i,day} = AL_{month} \times EF_{i,k} \times P_{i,m,day} \quad (6)$$

223 where EF represents the emission factor based on the technological evolution of the
224 plant, P is the temporal profile of emissions, based on the fraction of daily electricity
225 load out of the monthly total for specific sector.

226 **Vehicles (On-road transportation)** Daily vehicular emissions were estimated
227 utilizing the International Vehicle Emissions model (IVE) combined with the Gaode
228 live congestion index (Zhou et al., 2019; Kholod et al., 2016). The level of traffic
229 congestion was indicated by the additional time incurred during a trip under congested
230 conditions, expressed as a percentage relative to uncongested conditions (Huo et al.,
231 2022). The Gaode congestion index is available for over 350 cities in China, with a
232 temporal resolution of 5 minutes (<https://report.amap.com/index.do>, last visited on
233 October 2025). By integrating the congestion index with a Greenshield's traffic
234 density model (Yang et al., 2019), we estimated the traffic volume which serves as a
235 temporal allocation factor to calculate the daily emissions. This approach assumes that
236 vehicular activity data (e.g., mileage and fuel consumption) are accessible, albeit
237 typically with a lag in reporting, as such information is usually provided on an annual
238 basis. Consequently, the near-real-time emissions can be estimated based on the daily
239 variations of congested index and EFs compared to the previous year (Eq. 7):

240
$$E_{i,m,day} = \frac{(I_{day,year-1}) \times I_{day,(year-1)}^2 \times EF_{i,m,day,year}}{(I_{day,(year-1)}-1) \times I_{day,year}^2 \times EF_{i,m,day,(year-1)}} \quad (7)$$

241 where I is the Gaode traffic congestion index; and EF is the emission factor,
242 calculated by the IVE model. The input parameters of IVE such as the vehicle
243 population by type, registration dates, fuel types, and emission standards, can be
244 obtained from the transportation management departments of individual cities. These
245 historical data can be extrapolated to the present date utilizing the vehicle survival
246 curve, thereby bridging any gaps in the current information (Sun et al., 2020).

247 **Off-road Transportation** Off-road transportation was divided into five categories:
248 construction machinery, agricultural machinery, marine, railway, and aviation.
249 Emissions from construction machinery were estimated based on assumed daily



250 utilization rates derived from the operating rates of construction sites (Shen et al.,
251 2023; Huang et al., 2021). The daily usage of agricultural machinery was assumed to
252 correlate with the application of nitrogen fertilizers from agricultural sources (see the
253 description of agriculture as below). Emissions from railway, marine and aviation
254 sources were estimated using data from passenger/cargo turnover, individual ports and
255 commercial flights, respectively. These data were obtained from the China
256 Entrepreneur Investment Club (CEIC) (<https://www.ceicdata.com.cn>, last visited on
257 October 2025), Marine Traffic (<http://www.marinetraffic.com>, last visited on October
258 2025) and Flightradar24 databases (<http://www.flightradar24.com>, last visited on
259 October 2025) (Huo et al., 2022; Liu et al., 2020a).

260 **Residential sources** We followed Shao et al. (2023) and developed a Bayesian
261 hierarchical model to estimate daily heating energy consumption by fuel type, based
262 on two primary factors influencing residential energy consumption: temperature and
263 GDP. The daily temperature data were taken from ERA5 products provided by the
264 European Centre for Medium-Range Weather Forecasts (ECMWF)
265 (<https://cds.climate.copernicus.eu>, last visited on October 2025), while GDP from the
266 national statistics published quarterly by the National Bureau of Statistics
267 (<http://www.stats.gov.cn/>, last visited on October 2025). For the months without GDP
268 data, we assumed a linear relationship between GDP and the nighttime light index (Xu
269 et al., 2024), and applied the National Polar-orbiting Partnership Visible Infrared
270 Imaging Radiometer Suite (NPP-VIIRS, <https://www.earthdata.nasa.gov/>, last visited
271 on October 2025) provided by National Aeronautics and Space Administration
272 (NASA) to extrapolate the GDP for those months. We applied the gridded population
273 dataset (1km×1km) released by a database of the Chinese Academy of Sciences
274 (<https://www.resdc.cn/Default.aspx>, last visited on October 2025) for 2020. To
275 account for the effect of large-scale population migration, we integrated the
276 Population Migration Index (PMI) developed by Baidu (<https://qianxi.baidu.com/#/>,
277 last visited on October 2025). This index calculates the proportion of incoming
278 migrants relative to the local population.



279 **Agriculture** NH₃ emissions from fertilizer use can be largely influenced by
280 meteorological conditions, soil environment, and farming practices. In our previous
281 study, we quantified NH₃ emissions using dynamic EFs associated with those factors
282 (Zhao et al., 2020b). In this study, we expanded the methodology and estimated NH₃
283 emissions by using daily EFs. For livestock and poultry farming, we assumed that
284 daily NH₃ emissions were associated with temperature, while those for human
285 excretion associated with both temperature and PMI.

286 **2.3 Air quality modeling**

287 To evaluate the near-real-time emission estimate, we used the Community Multiscale
288 Air Quality (CMAQ v5.1) model developed by US Environmental Protection Agency
289 (<https://www.epa.gov/cmaq>, last visited on October 2025), to simulate the PM_{2.5} and
290 O₃ concentrations in Jiangsu. Four months (January, April, July, and October) in 2022
291 were selected as the simulation periods, with a spin-up time of 7 days for each month
292 to reduce the impact of the initial condition on the simulation. As shown in
293 Supplementary Figure S1, three nested domains (D1, D2, and D3) were applied with
294 the horizontal resolutions at 27, 9, and 3 km, respectively, and the most inner D3
295 covered Jiangsu and parts of the YRD region including Shanghai, northern Zhejiang,
296 and eastern Anhui. The Multi-resolution emission inventory of China (MEIC, <http://http://meicmodel.org.cn/>, last visited on October 2025) was applied for D1, D2, and
297 the regions out of Jiangsu in D3 (Zheng et al., 2018), and the provincial-level
298 near-real-time emission estimate was applied for Jiangsu in D3. The Carbon Bond
299 Mechanism (CB05) and AERO5 mechanisms were used for the gas-phase chemistry
300 and aerosol module, respectively.

302 The meteorological field for the CMAQ was obtained from the Weather Research and
303 Forecasting model (WRF v3.4, <https://www.mmm.ucar.edu/models/wrf>, last visited on
304 October 2025). Meteorological initial and boundary conditions were obtained from
305 the National Centers for Environmental Prediction (NCEP,
306 <https://psl.noaa.gov/data/reanalysis/reanalysis.shtml>, last visited on October 2025)
307 datasets. Ground observations at 3-h intervals were downloaded from National



308 Climatic Data Center (NCDC, <ftp://ftp.ncdc.noaa.gov/pub/data/noaa/isd-lite/>, last
309 visited on October 2025). Statistical indicators including bias, index of agreement
310 (IOA), and root mean squared error (RMSE) were used to evaluate the WRF
311 performance (Gu et al., 2023). The discrepancies between simulations and ground
312 observations were within an acceptable range (Supplementary Table S1).

313 We collected ground observation data of hourly PM_{2.5} and O₃ concentrations at the
314 110 state-operating air quality monitoring stations within Jiangsu
315 (<https://data.epmap.org/page/index>, see the station locations in Figure S1, last visited
316 on October 2025). Correlation coefficients (R), normalized mean bias (NMB) and
317 normalized mean errors (NME) between observation and simulation for each month
318 were calculated to evaluate the performance of CMAQ modeling.

319 We further compared the modeling performance using provincial-level emission
320 estimate in D3 with that using MEIC. MEIC was currently available only for 2020. To
321 avoid the bias from the total emission level, we adjusted the total emissions of various
322 species in 2020 MEIC to be consistent with our estimates, retaining the
323 spatiotemporal and sector distribution of the emissions.

324 **2.4 Removing meteorological influence on PM_{2.5} and O₃ concentrations**

325 To explore the influence of anthropogenic emission changes on the variability of
326 PM_{2.5} and O₃ levels in 2022, we removed the impact of varying meteorological
327 conditions by employing a stepwise multiple linear regression (MLR) model (Li et al.,
328 2021). The surface daily concentrations of O₃ and PM_{2.5} were taken from the Tracking
329 Air Pollution in China (TAP, <http://tapdata.org.cn/>, last visited on October 2025) with
330 a horizontal resolution of 1 km×1 km (Geng et al., 2021). We incorporated nine
331 meteorological variables from the ERA5 database at a resolution of 0.25°×0.25°,
332 considered as the potential covariates for O₃ and PM_{2.5}. They were 10-meter zonal and
333 meridional wind speeds, temperature, boundary layer height, sea level pressure, cloud
334 cover, precipitation, relative humidity, and dew point temperature. These variables
335 were then scaled to a 3km×3km grid system by bilinear interpolation. To prevent
336 overfitting, we conducted MLR with the three most influential meteorological



337 parameters to estimate the variability of daily PM_{2.5} and maximum daily 8-hour
338 average (MDA8) O₃ concentration for each grid cell. Anomaly (the difference
339 between the raw data and the moving average of 30 days around) of air pollutant
340 concentrations and meteorological factors were used in the model, to exclude the
341 effect of monthly variability. Residuals that cannot be explained by the meteorological
342 variables were assumed to be attributed to anthropogenic emission changes (Li et al.,
343 2020). The results could be interpreted as the sensitivity of air pollutant concentration
344 to the daily emission anomalies from the annual average value.

345 To evaluate the MLR performance, we collected daily PM_{2.5} and O₃ concentrations at
346 the above-mentioned 110 air quality monitoring stations in Jiangsu (Figure S1), and
347 the R and NMB between observation and MLR were calculated.

348 **2.5 Examining the response of MDA8 O₃ and PM_{2.5} concentration to changing
349 daily emissions**

350 **2.5.1 XGBoost model**

351 XGBoost model is an advanced and scalable machine learning framework based on
352 gradient-boosted decision trees, widely recognized for its efficiency in handling
353 structured data and modeling complex nonlinear relationships (Requia et al., 2020;
354 Wang et al., 2023). XGBoost excels at processing high-dimensional spatiotemporal
355 datasets, such as gridded emission inventories, by effectively capturing interactions
356 among heterogeneous emission sources and temporal dependencies. Moreover, the
357 inherent interpretability features facilitate seamless integration with explainable AI
358 tools (e.g., SHapley Additive exPlanations (SHAP) to quantify the marginal
359 contribution of each input feature to individual model predictions), enabling rigorous
360 attribution analysis of air pollutant concentration variability (Zhao et al., 2025). The
361 SHAP value is calculated with following equation:

$$362 \quad y_i = y_{base} + f(X_{i,1}) + f(X_{i,2}) + \dots f(X_{i,n}) \quad (8)$$

363 where y_i is the predicted value of the model for the i th sample; $f(X_{i,n})$ is the



364 contribution of the nth eigenvalue in the ith sample to the final predicted value, with
365 positive or negative representing that the eigenvalue makes the predicted value
366 increase or decrease; and y_{base} is the baseline value of the predicted outputs for all
367 types of predictions, representing the average prediction results for each category
368 without the influence of any eigenvalue.

369 **2.5.2 Anthropogenic effects on PM_{2.5} and MDA8 O₃ variability**

370 The XGBoost-SHAP modeling framework was implemented at the horizontal
371 resolution of 3km×3km to capture the emission-concentration relationship. XGBoost
372 regression models were independently trained for each grid cell. January and July
373 were selected as typical months for ambient PM_{2.5} and O₃, respectively. Daily time
374 series of 20 pollutant-sector combinations (4 pollutant (SO₂, NO_x, NMVOCs, PM_{2.5})
375 × 5 sectors (Power, Industry, On-road (Vehicles), Off-road, Residential) except for
376 tiny On-road SO₂, and agricultural NH₃) were set as predictors, and
377 anthropogenic-driven variability of PM_{2.5} or O₃ concentrations as target variables.
378 Similarly, the emission inputs were treated as anomaly (the difference between the
379 current day's emissions and the moving average of 30 days around). A 10-fold
380 cross-validation was applied (80% training and 20% testing), and the bias and
381 correlation coefficient (R) were calculated to evaluate the model performance (Xiao et
382 al., 2018).

383 SHAP values were calculated for each emission feature using the tree explainer
384 algorithm, quantifying contributions of pollutant-sector combinations to variability of
385 daily anthropogenic-driven concentrations. Note that SHAP values represented the
386 deviation of individual predictions from the baseline expectation. Positive values
387 indicated emission features that elevated pollutant concentrations above the baseline,
388 while negative values indicated features that reduced concentrations below the
389 baseline. Aggregation of daily SHAP values for various pollutant-sector combinations
390 produced the daily-level contribution of total anthropogenic emissions to the changing
391 ambient concentration, and the daily-level contributions could then be aggregated to



392 the monthly level.

393 **3. Results and discussions**

394 **3.1 Anthropogenic air pollutant emissions**

395 **3.1.1 Total air pollutant emissions in 2022**

396 The total anthropogenic emissions of SO₂, NO_x, PM_{2.5}, NMVOCs, and NH₃ in
397 Jiangsu for 2022 were estimated at 246, 727, 298, 1186, and 377 Gg (Supplementary
398 Figure S2), which were respectively reduced by 17%, 33%, 18%, 7%, and 11%
399 compared with those in 2019 (Gu et al., 2023). Our estimates indicated that the
400 reduction rate of SO₂ emissions was much lower between 2019 and 2022 than that at
401 53% between 2015 and 2019. In particular, the emissions from the power sector were
402 estimated to decline only 7% during 2019-2022. The result confirmed that the
403 abatement of SO₂ emissions have been clearly decelerated following the full
404 implementation of ultra-low emission retrofits, suggesting that the potential of further
405 reduction of SO₂ emissions for power sectors has become more limited. More energy
406 structure adjustment instead of end-of-pipe controls is needed for the sector.

407 In contrast to SO₂, the emissions of NO_x and PM_{2.5} were estimated to decline faster
408 during 2019-2022 than 2015-2019. Industrial sectors contributed largely to these
409 reductions, with the emission declining 27% and 22% for NO_x and PM_{2.5},
410 respectively (Figure S2). These reductions reflected expansion of intensified pollution
411 control policies from power to other sectors, particularly the ultra-low emission
412 standards implemented for steel (2019) and cement industries (2020)
413 (<https://sthjt.jiangsu.gov.cn/>, last visited on October 2025). By 2022, Jiangsu province
414 had implemented ultra-low emission retrofits in over 80% of iron & steel enterprises
415 and approximately 60% of cement clinker production lines (DEE, 2023). However,
416 slower progress of emission controls in coking, glass, and chemical industries
417 highlighted substantial emission reduction potential in these non-electrical industrial
418 sectors. Meanwhile, the NO_x emissions of transportation were estimated to decline by



419 41% from 2019 levels (53% for light-duty gasoline vehicles), driven mainly by the
420 nationwide implementation of China VI vehicle emission standard and increasing
421 penetration of renewable energy vehicles.

422 NMVOCs, as critical precursors of both secondary $PM_{2.5}$ and O_3 formation, exhibited
423 a slower decline in emissions and have emerged as the priority of emission controls in
424 Jiangsu (Figure S2). Industrial activities dominate NMVOCs emissions in Jiangsu,
425 contributing 68% of the provincial total emissions. It resulted from the heavy
426 dependence of the province on chemical industries. For example, the province
427 accounted for over 40% of national pesticide active ingredient and dye production.
428 Notably, more than 60% of small-scale chemical enterprises persisted in utilizing
429 solvent-based coatings, inks, and adhesives with high-VOCs content (Simayi et al.,
430 2022; Hu et al., 2024). Furthermore, recent expansions in solvent consumption and
431 chemical output within large-scale enterprises along the Yangtze River have largely
432 offset the emission reductions through improvement of manufacturing and pollution
433 control technologies (Li et al., 2019). Consequently, intensified emission controls
434 should be urgently required for targeting key industrial sectors and critical regions for
435 NMVOCs reduction. Agricultural NH_3 emissions in Jiangsu have experienced a
436 decline of 14% during 2019-2022, primarily attributed to reduced nitrogen fertilizer
437 usage. However, the absence of effective NH_3 control measures prevented further
438 substantial reduction of emissions for the sector (Zhou et al., 2023; Zhao et al., 2022).

439 3.1.2 Daily emission variability for air pollutants in 2022

440 Figure 2 show the daily variability of total and sectoral emissions of various pollutants
441 (SO_2 , NO_x , $PM_{2.5}$, NMVOCs, and NH_3) in 2022, respectively (the time series of
442 emissions (NO_x as an example) for all the involved source categories are provided in
443 Supplementary Figure S3). The results revealed distinct seasonal emission patterns of
444 air pollutants driven by anthropogenic activities and/or meteorological conditions.

445 The emissions of SO_2 and primary $PM_{2.5}$ followed the seasonal patterns of fossil
446 energy consumption (Yun et al., 2021), with clear peaks in winter (from December to



447 February) associated with the substantial coal combustion for residential heating and
448 elevated industrial energy demand (Geng et al., 2021; Zhan et al., 2023). Regarding
449 NO_x, transportation has become the primary contributor to the emissions along with
450 improved emission controls from the power and industrial sectors. Following the
451 lifting of COVID-19 lockdown since June 2022, moreover, residents exhibited a
452 strong desire to travel, which enhanced the emissions from transportation. Compared
453 to the spring (from March to May), NO_x emissions from transportation increased 12%
454 during the summer (from June to August), consistent with the elevated population
455 mobility (Supplementary Figure S4). Additionally, the NO_x emission peak in March
456 reflected the resumption of industrial production and construction activities after the
457 Chinese New Year. The area of construction for residential and commercial buildings
458 increased 56% from February to March, with these activities heavily dependent on
459 diesel-powered machinery (Yang et al., 2015; Cliff et al., 2023). The NMVOCs
460 emissions were the largest in summer. Enhanced volatilization of solvents and
461 industrial chemicals by the warmer temperatures resulted in a 22% growth of summer
462 emissions compared to spring. Similar to NO_x, the NMVOCs emissions in March
463 rebounded with a 17% growth compared to February, reflecting the resumption of
464 coating, printing, and petrochemical industries. NH₃ were closely associated with
465 farming cycles, peaking during Spring sowing and Autumn harvesting periods.

466 Notably, the province has made great efforts on reducing emissions during the period
467 with heavy pollution weather (DEE, 2022). Compared to August 2022, mandatory
468 restrictions on coal-fired boilers and industrial plants for September resulted in an 11%
469 reduction of coal consumption for major industrial sectors, leading to a decline of 7%,
470 10%, 15%, and 12% for anthropogenic emissions of SO₂, NO_x, PM_{2.5}, and NMVOCs,
471 respectively. This demonstrated the effectiveness of pollution control measures
472 conducted by the government on counteracting pollution episodes around August and
473 September, despite persistent meteorological challenges (Wang et al., 2023). However,
474 subsequent emission rebounds in winter for SO₂ (+24% compared with those in
475 Autumn) and PM_{2.5} emissions (+19%) underscored the limitation of seasonal control



476 strategies for combustion-derived pollutants, emphasizing the imperative for clean
477 energy promotion to achieve sustainable emission abatement.

478 In April 2022, a great reduction in air pollutant emissions was estimated. Compared
479 with March, the emissions of SO₂, NO_x, PM_{2.5}, and NMVOCs decreased by 11%, 8%,
480 6%, and 12% respectively. This abrupt decline was temporally associated with the
481 COVID-19 induced lockdown implemented in Shanghai (March 28-June 1, 2022).
482 The lockdown substantially disrupted industrial production, transportation activities,
483 and daily routines in neighboring Jiangsu Province. The results showed that
484 short-term public health incidents exerted profound impact on air pollutant emissions
485 (Zhang et al., 2024; Ma et al., 2023).

486 **3.1.3 High-resolution maps of air pollutant emissions**

487 Based on the real-time geospatial information from the POI system (e.g., quarterly
488 updated road networks, land use types, and monthly revised construction sites), we
489 achieved the evolving spatial pattern of daily air pollutant emissions with a horizontal
490 resolution of 3 km×3 km. Figure 3 presents the spatial distribution of daily average
491 emissions of major sectors in Jiangsu Province for 2022. We selected NO_x as an
492 example to illustrate the sector heterogeneity. The NO_x emissions from power,
493 industrial, vehicle, off-road transportation and residential sources in Jiangsu were
494 calculated at 144, 109, 247, 183 and 45 Gg respectively. Aviation emissions (less than
495 1% of total NO_x) were excluded due to their tiny contribution to the total emissions.

496 The spatial pattern of emissions was closely associated with corresponding
497 anthropogenic activities. Agricultural machinery emissions were predominantly
498 located in northern agricultural zones and coastal areas, correlating with the
499 spatiotemporal distribution of farming activities. In contrast, emissions from other
500 sources were more concentrated in the southern cities, especially along the Yangtze
501 River with the most abundant power and industrial plants. The NO_x emissions from
502 five cities in southern Jiangsu (Nanjing, Suzhou, Wuxi, Changzhou, Zhenjiang)
503 accounted for 59% and 63% of provincial power and industrial emissions,



504 respectively. On-road transportation emissions demonstrated a strong dependence on
505 the road network. Nanjing and Xuzhou, as critical national railway transportation hubs,
506 contributed 24% and 13% of provincial NO_x emissions from railways (Wang et al.,
507 2016). In addition, Suzhou contributed 29% of provincial marine emissions, attributed
508 to its pivotal role in Yangtze River Delta inland waterway logistics (Shen et al., 2021).
509 Unsurprisingly, the residential NO_x emissions were closely correlated with the
510 population density.

511 **3.1.4 Assessment of monthly variability**

512 Figure 4 compares the monthly distributions of SO₂, NO_x, and PM_{2.5} emissions
513 estimated in this study with those in MEIC, as well as those of provincial averages of
514 ambient concentrations of corresponding species obtained from the state-operating
515 observation sites in Jiangsu. Due to the unavailability of MEIC for the year 2022, we
516 used the result for 2020 instead.

517 For SO₂ (Figure 4a) and PM_{2.5} (Figure 4e), our analysis demonstrated a close
518 agreement between monthly variation in emissions and that in observed concentration
519 across Jiangsu Province. The near-real-time emission estimates effectively captured
520 the short-term fluctuations, including the abrupt reduction in April associated with
521 COVID-19 lockdown and the seasonal change from the temporary pollution control
522 measures in autumn. These results partly justified the capability of the approach to
523 track the effect of changing anthropogenic activities on air pollutant emissions.
524 Meanwhile, we found contrary monthly distributions between NO_x emissions and the
525 observed concentration of NO₂ (Figure 4c). The largest emissions were estimated in
526 summer months but the lowest concentrations were observed for the same months
527 across the year. This inconsistency likely resulted from following factors. Increased
528 transportation activity during summer, particularly mobility rebound after lockdown,
529 elevated NO_x emissions, while NO₂ was substantially consumed for O₃ formation
530 through photochemical reactions. In winter, there was more NO₂ accumulation in the
531 atmosphere with slower photochemical reactions and reduced boundary layer heights



532 (Ding et al., 2015; Wang et al., 2012). In addition, we found a similar correlation
533 between PM_{2.5}-NO₂ in monthly trends, implying the importance of controlling NO_x
534 emissions in reducing PM_{2.5} pollution.

535 Similar monthly distribution of emissions were found for the national (MEIC) and
536 provincial emission estimates (this work), implying regular patterns of monthly
537 anthropogenic activities could be captured by both inventories. Nevertheless,
538 disparities existed in the overall emission totals and sector distributions between the
539 two inventories. For instance, the contributions of industry to provincial emissions of
540 SO₂ and NO_x were estimated at 45% and 15% in this work, greatly different from the
541 MEIC estimation at 72% and 41%, respectively. These discrepancies might be
542 attributed to that the national inventory (MEIC) for 2020 has not yet fully included the
543 information of emission control technology upgrades (e.g., ultra-low emission
544 retrofits) in the industrial sector. Taking the sintering process in the steel industry as
545 an example, our facility-level estimations indicated that the average emission factors
546 for SO₂, NO_x, and PM_{2.5} were 0.143 kg/t, 0.228 kg/t, and 0.037 kg/t, respectively,
547 much lower than the recommended values of 1.34 kg/t, 0.55 kg/t, and 2.52 kg/t from
548 the guidelines for development of national emission inventory (He et al., 2018).

549 Substantial discrepancies were revealed for off-road transportation of SO₂ emissions.
550 The provincial SO₂ emission estimate from marine (12,877 metric tons) were almost
551 three times of that by MEIC (4,690 metric tons). As a major freight hub in the eastern
552 coastal region of the country, Jiangsu Province played a pivotal role in marine
553 transportation, and approximately 60% of vessels utilized heavy oil with high-sulfur
554 content as fuel (Dong et al., 2025). Application of national average EFs for the sector
555 might lead to underestimation in emissions. Furthermore, the national inventory
556 ignored the emissions from passing vessels at ports. Inclusion of such vessels would
557 increase the SO₂ emissions in the Yangtze River Delta region by a factor of 2.3
558 (Zhang et al., 2017). As power and industrial sectors have gradually completed
559 ultra-low emission retrofits, marine emissions with less stringent controls may
560 become more important in the future, requiring greater efforts on fuel quality



561 improvement and stricter emission controls.

562 **3.2 Impacts of short-term lockdown on changes in emissions**

563 From March 28 to June 1 in 2022, Shanghai, the largest megacity in YRD and the
564 national center of economy, finance, manufacturing, and maritime trade in China,
565 implemented stringent COVID-19 lockdown measures that suspended intercity
566 mobility and industrial production and kept only essential logistics. This
567 unprecedented lockdown not only disrupted social and economic activities of
568 Shanghai, but also brought substantial effects for neighboring regions. Jiangsu
569 Province, a highly industrialized region adjacent to Shanghai, experienced severe
570 disruptions across service sectors, manufacturing supply chains, and maritime
571 logistics, resulting in substantial declines in energy consumption, industrial output,
572 and transportation activities. To further quantify the lockdown effect on air pollutant
573 emissions, we conducted a comparative analysis between two periods: the
574 lockdown-affected period (April-May 2022) and the post-pandemic period, the same
575 months one year later (April-May 2023).

576 The first column of Figure 5 (a1, b1, c1, d1) illustrates the variability in daily
577 emissions of NO_x, SO₂, PM_{2.5}, and NMVOCs in Jiangsu during April-May 2022
578 (lockdown period) versus 2023 (recovery period), as well as the difference between
579 the two periods. The emission differences (calculated as the relative change compared
580 to the 2023 level) reached 8%, 6%, 6%, and 10% for these air pollutants, respectively.
581 The most substantial decline in pollutant emissions occurred in April 2022, with a
582 gradually diminishing difference in May. However, the emissions by the end of May
583 2022 did not reach the level of recovery period in May 2023, reflecting the effect of
584 temporary measures on reducing economic activities even after the lifting of the
585 lockdown. The full economy recovery was delayed until 2023 when pandemic
586 restrictions were completed lifted (Li et al., 2023).

587 The second and third columns of Figure 5 (a2-d2 and a3-d3) illustrate the
588 contributions of various pollution source categories to the differences in emissions



589 between April-May of 2022 and 2023. Agricultural production remained basically
590 unaffected by the pandemic, thus the emission changes from agricultural machinery
591 were not included. The total reduction in NO_x emissions was 9,970 metric tons,
592 predominantly attributed to transportation sources. The sector contributed to over 70%
593 of the emission reduction, including on-road transportation (15%), construction
594 machinery (27%), marine (19%), railway (5%), and aviation (4%). This result is
595 consistent with the findings on the effect of the 2020 COVID-19 lockdown (Lv et al.,
596 2020; Zhao et al., 2020a). However, there was a slight rebound in motor vehicle
597 emissions in May, which could be associated with basic everyday living and working
598 needs. Notably, construction machinery and marine were more affected by the
599 lockdown, attributable to construction material shortages (39% fewer of constructing
600 and building activities) and disrupted inland waterway logistics (20% less of port
601 throughput). Compared with transportation, the reduction of NO_x emissions from the
602 power (1,955 metric tons) and the industrial sector (1,202 metric tons) were smaller.
603 The decline in industrial electricity demand reduced the fossil fuel consumption and
604 thereby the NO_x emissions from the power sector. During industrial shutdowns and
605 production restrictions caused by the epidemic, frequent start-ups and shutdowns of
606 production and pollution control equipment resulted in a clear decline in NO_x
607 removal efficiency compared with normal operation condition of selective catalytic
608 reduction (SCR) systems. Previous measurements found that the average NO_x
609 removal efficiency of coal-fired units in iron & steel production enterprises decreased
610 from 78% to 61% (Shao et al., 2023), which to some extent offset the emission
611 reduction effect of industrial sources due to production restrictions.

612 SO₂ emission reductions predominantly originated from power (521 metric tons, 21%)
613 and industrial sectors (1,710 metric tons, 68%). For PM_{2.5}, transportation contributed
614 56% to the total reduction of 3,583 metric tons, with the contributions from on-road
615 transportation, construction machinery, marine, railway, and aviation accounting for
616 8%, 18%, 14%, 9%, and 7%, respectively. The emission reductions of NMVOCs were
617 estimated at 20,170 metric tons. The contribution of industrial sources reached 93%,



618 largely due to a 64% decline in crude oil processing in Jiangsu Province compared to
619 2023, as well as the substantial declines in the production of chemical products (e.g.,
620 27% less in chemicals fibers and 65% less in ethylene manufacturing, NBS, 2023).
621 The results emphasized the lockdown impact on petrochemical industries reliant on
622 cross-regional material flows. In contrast, the emissions from residential sector were
623 larger for the lockdown period, with its coal consumption 7% more than that in
624 recovery period one year later, likely driven by the enhanced heating/cooking
625 demands during mobility restrictions.

626 In a summary, the results revealed complicated and diverse interventions of public
627 health incidents on energy use and activities for different sectors. The near-real-time
628 techniques developed in this work proved capable to capture the fast response of air
629 pollutant emissions to the short-term measures conducted during unexpected incidents,
630 and to clearly identify the driving sectors of emission changes compared to the normal
631 conditions.

632 **3.3 Evaluation of the near-real-time emission estimates with air
633 quality simulation**

634 The near-real-time estimates of provincial emissions were evaluated with air quality
635 simulation with CMAQ. To assess model performance, the observed concentrations of
636 hourly SO_2 , NO_2 , $\text{PM}_{2.5}$, and MDA8 O_3 were compared with the simulations based on
637 the provincial-level near-real-time emission estimates and MEIC for the selected four
638 months of 2022, as summarized in Supplementary Table S2. Overall, the simulation
639 with the provincial emission estimates shows acceptable agreement with the
640 observations, with the annual means of NMB and NME ranging -37.1% – 24.1% and
641 33.7% – 53.5% for SO_2 , -20.2% – 27.0% and 15.9% – 36.2% for NO_2 , -18.6% – 10.8%
642 and 37.5% – 62.5% for $\text{PM}_{2.5}$, and -41.2% – -23.1% and 32.7% – 49.3% for O_3 . The
643 analogous numbers for MEIC were -33.4% – 25.5% and 40.9% – 51.8% for SO_2 , -19.9%
644 – 35.6% and 22.3% – 55.1% for NO_2 , -8.6% – 25.2% and 37.5% – 52.5% for $\text{PM}_{2.5}$,
645 and -39.9% – -28.1% and 44.3% – 54.5% for O_3 , respectively. Most of the NMB and



646 NME were within the recommended criteria ($-30\% \leq NMB \leq 30\%$ and $NME \leq 50\%$,
647 Emery et al., 2017). Better performance was achieved using the provincial emission
648 estimates developed in this work, implying the benefit of applying the refined
649 emission data on high-resolution air quality simulation.

650 Figures 6 and 7 compares the simulated daily $PM_{2.5}$ and O_3 concentrations based on
651 the provincial (this work) and national emission estimates (MEIC) against
652 observations (results for SO_2 and NO_2 are shown in Supplementary Figures S5 and S6,
653 while spatial distributions for all the four pollutants are provided in Supplementary
654 Figures S7-S10). Compared to MEIC, the provincial-scale emission estimates
655 demonstrated better model performance in capturing the daily variability of pollutant
656 concentrations. The greater correlation coefficients (R) between simulated and
657 observed concentrations based on the near-real-time estimates indicated a remarkable
658 improvement for all the involved air pollutants (Table S2).

659 For $PM_{2.5}$, the improvement in model performance based on the provincial emission
660 estimates was particularly prominent concerning the impact of the COVID-19
661 lockdown measures in April. As shown in Figure 6, the near-real-time approach more
662 accurately captured the decline in $PM_{2.5}$ level from reduced emissions. As a
663 comparison, notable overestimation of $PM_{2.5}$ concentration occurred for simulation
664 with MEIC. As a national emission inventory, MEIC commonly applied the temporal
665 profiles of activity data for various sectors for the whole country, thus could
666 insufficiently track the effect of temporary and unexpected events on emissions, such
667 as the city lockdown. For O_3 , despite of the underestimation for both emission
668 inventories, application of the near-real-time provincial estimates not only reduced the
669 underestimation compared to MEIC but also better captured the variability of O_3
670 concentration driven by short-term emission fluctuations. These results collectively
671 demonstrated the improvement in model performance and advantage of near-real-time
672 emission estimates to support high-resolution air quality simulation.

673



674 **3.4 Impact of daily emission change on the variability of PM_{2.5} and O₃**

675 **concentrations**

676 **3.4.1 Anthropogenic-driven contributions to variability of PM_{2.5} and MDA8 O₃**

677 **concentrations**

678 Figure 8 presents the contributions of the changing daily emissions to the monthly
679 variability of PM_{2.5} and MDA8 O₃ concentrations based on the MLR model. The
680 model performance was assessed with observed PM_{2.5} and O₃ concentrations
681 (Supplementary Figure S11). The simulated concentrations were strongly correlated
682 with observational data, with the correlation coefficient (R) of 0.79 for PM_{2.5} and 0.88
683 for MDA8 O₃. The validation indicated satisfying performance of MLR in capturing
684 provincial air quality variability.

685 The anthropogenic-driven variability of PM_{2.5} concentration was basically consistent
686 with the temporal variation of estimated emissions. As shown in Figure 8a, the
687 abundant emissions in January resulted in a prominent enhancement of 12.7 µg/m³ for
688 PM_{2.5} concentration, followed by December (1.8 µg/m³) and June (1.6 µg/m³). In
689 particular, the enhancement of June was driven largely by the post-pandemic
690 economic recovery, as discussed in in Section 3.2. For most warm months (April to
691 October, except June), negative impacts of anthropogenic activities on PM_{2.5} level
692 were found, ranging 1.1 – 4.2 µg/m³. Clear decline of PM_{2.5} due to emission change
693 was also found in February (5.5 µg/m³), resulting probably from the greatly reduced
694 human activities (industry and transportation) during the Chinese New Year holiday.
695 The PM_{2.5} growth occurred during winter heating period highlighted the necessity of
696 accelerating transition of clean household energy and improving management of
697 industrial production after the short-term lockdowns.

698 The variation of anthropogenic emissions was found to elevate O₃ concentrations in
699 most months of the year, particularly for warm seasons (Figure 8b). The
700 enhancements during March-August ranged 0.8 – 3.8 µg/m³, suggesting the important
701 role of human activities in aggravating O₃ pollution. High temperature in summer
25



702 promoted the emissions of temperature-dependent O₃ precursors, particularly
703 NMVOCs from various sources (Figure 2d). In addition, the NO_x emissions from
704 certain were elevated in warm seasons, e.g., those from off-road machinery in the
705 summer harvest season (Figure 2a). The growing abundance of precursors, together
706 with high temperature, enhanced the photochemical production rate of O₃.

707 However, the anthropogenic emissions during winter demonstrated a net negative
708 contribution to surface O₃ concentrations (e.g., -6.2 and -2.4 µg/m³ for November and
709 December, respectively), indicating a shift in the chemical regime of O₃ formation.
710 This phenomenon primarily resulted from enhanced NO_x titration amplified by
711 elevated NO_x level. Simultaneously, reduced NMVOCs emissions and diminished
712 photochemical activity restricted the efficiency of radical-driven O₃ production. The
713 resulting O₃-depleting reactions overwhelmed potential formation mechanisms,
714 leading to the estimated negative contribution from anthropogenic emissions. This
715 pattern contrasted sharply with the net positive effect of anthropogenic activities in
716 summer months, and underscored the complex season-dependent response of O₃ level
717 to the changing precursor emissions.

718 **3.4.2 Impact of fluctuations in anthropogenic emissions by precursor and sector
719 on PM_{2.5} and MDA8 O₃ concentrations**

720 The impacts of anthropogenic emission fluctuations on variability of PM_{2.5} and O₃
721 concentrations were quantified by precursor and sector, with a machine learning
722 framework integrating XGBoost and SHAP analysis. Derived from the 10-fold cross
723 validation, the correlation coefficient (R) between machine learning prediction and
724 observation reached 0.78 and 0.81 for daily PM_{2.5} and MDA8 O₃, respectively,
725 suggested satisfying capability of the machine learning framework in predicting the
726 anthropogenic-driven variability of PM_{2.5} and O₃ concentrations (Supplementary
727 Figure S12).

728 Figure 9a and 9b illustrates the contributions of changing emissions from different
729 pollutant-sector combinations to the variability of PM_{2.5} concentration in January and



730 that of MDA8 O₃ in July, respectively. The temporal variability of PM_{2.5} level
731 attributable to anthropogenic emission changes was in general consistent with that of
732 observed surface PM_{2.5} concentration (Figure 9a). For O₃, there existed some
733 discrepancy between the temporal distribution of anthropogenic-driven variability and
734 observed concentration in summer. This discrepancy may be attributed to the
735 substantial impacts of meteorological conditions and biogenic VOCs emissions on O₃
736 formation (Gu et al., 2023).

737 Among all the pollutant-sector combinations, fluctuations in agricultural NH₃
738 emissions accounted for 67.3% of the variability of PM_{2.5} concentrations in January,
739 followed by off-road NO_x (12.9%) and residential PM_{2.5} emissions (4.9%). The
740 contribution of NH₃ emission variation significantly exceeded those of NO_x (17.7%),
741 PM_{2.5} (10.8%), and SO₂ (4.2%), suggesting that Jiangsu may be transitioning to an
742 NH₃-rich regime following substantial reductions in SO₂ and NO_x emissions (Zhao et
743 al., 2020b). Therefore, agricultural NH₃ control has become the priority of the strategy
744 design for PM_{2.5} pollution alleviations, compared to traditional NO_x abatement. The
745 fluctuations in VOC-Industry contributed to 48.5% of the variability of MDA8 O₃
746 concentrations in July, followed by off-road VOCs (9.7%) and NO_x emissions (8.9%).
747 In total, the NMVOCs accounted for 69.7% of the anthropogenic-driven variability of
748 O₃ concentration, exceeding the contributions from NO_x (14.5%), PM_{2.5} (11.0%), and
749 SO₂ (4.9%). The positive contribution of NO_x to MDA8 O₃ indicated that the O₃
750 formation mechanism in Jiangsu may be shifting from a VOCs-limited regime
751 towards a transitional or NO_x-limited regime. Regarding the sector contributions with
752 various species aggregated, the agricultural emission fluctuations contributed most to
753 anthropogenic-driven variability of PM_{2.5} concentration (67.3%, Figure 9c), while
754 industrial activities contributed most to that of O₃ concentration (54.8%, Figure 9d).
755 Notably, off-road transportation emerged as an important contributor to both
756 pollutants (15.6% for PM_{2.5} and 24.4% for O₃), providing clear evidence for policy
757 making of coordinating control of PM_{2.5} and O₃ pollution.



758 4. Conclusion remarks

759 In this study, we incorporated near-real-time activity data from multiple sources and
760 developed a method for continuously estimating the regional daily air pollutant
761 emissions of anthropogenic origin. We then applied this method to estimate the
762 spatiotemporal evolution of emissions in Jiangsu Province, a typical developed area in
763 eastern China, with a particular focus on the period during the COVID-19 lockdown
764 in 2022 and the corresponding phase after the lifting of restrictions in 2023. Finally,
765 we constructed a rapid assessment approach that utilized machine learning algorithms
766 to quantify the impact of fast changing emissions on variability of daily air quality.
767 Our research indicated that emission controls have played a crucial role in abatement
768 of air pollutant emissions. The provincial emissions of SO_2 , NO_x , $\text{PM}_{2.5}$, NMVOCs,
769 and NH_3 decreased 17%, 33%, 18%, 7%, and 11%, respectively, from 2019 to 2022.
770 Implementation of ultra-low emission retrofits for industrial sectors has proven
771 effective in reducing primary $\text{PM}_{2.5}$ and NO_x emissions. However, there is an urgent
772 need to enhance NMVOCs emission control in key industrial sectors and areas. We
773 identified distinct temporal variabilities of emissions for various air pollutants. The
774 emissions of SO_2 and $\text{PM}_{2.5}$ were influenced greatly by fossil fuel consumption
775 pattern, while NO_x emissions were increasingly dominated by that of transportation.
776 The NMVOCs emissions peaked in the summer and declined in winter, followed by a
777 rebound in emissions after the Chinese New Year. Our comparative analysis indicated
778 that the emissions of NO_x , SO_2 , $\text{PM}_{2.5}$, and NMVOCs in Jiangsu during the
779 COVID-19 lockdown of Shanghai in April-May 2022 were respectively 8%, 6%, 6%,
780 and 10% smaller than those in the same months of 2023. Transportation was identified
781 as the primary contributors to the reductions in NO_x and $\text{PM}_{2.5}$ emissions, while
782 industry accounted for 93% of the reduction in NMVOCs, closely associated with the
783 disrupted cross-regional product supply chains. Indicated by the contributions of
784 changing emissions from pollutant-sector combinations to the variability of $\text{PM}_{2.5}$ and
785 O_3 levels, reducing agricultural NH_3 emissions should be critical for $\text{PM}_{2.5}$ pollution
786 alleviation, and off-road transportation has become a priority target for coordinating



787 control of both PM_{2.5} and O₃ pollution. The outcomes demonstrated the importance of
788 near-real-time techniques on tracking the fast-changing air pollutant emissions,
789 identifying the driving factors of air pollution variability, and supporting the policy
790 making of air quality management.

791 The limitations of this work existed mainly in the near-real-time information of
792 multiple sources and the rapid assessment of air quality variability. For instance,
793 CEMS covered only relatively big point sources, thus we had to assume that the small
794 and fugitive sources followed similar variability of emissions with point sources. As
795 CEMS only covers SO₂, PM_{2.5}, and NO_x, the use of electricity consumption data for
796 NMVOCs may introduce substantial uncertainty. Future improvement in online
797 monitoring of NMVOCs will enhance the estimation of temporal variation of
798 emissions. Moreover, the machine learning process ignored the contributions from
799 regional transport, which could result in some bias in analyzing the impacts of
800 anthropogenic emissions on air quality. However, in contrast to time-consuming
801 numerical modeling, machine learning offered a rapid and reliable assessment of the
802 impact of daily emission changes on air quality, which exactly addressed the
803 requirement of air quality management, and was recommended in future policy
804 making of air pollution controls.

805 **Data availability**

806 The gridded emission data for Jiangsu Province 2022-2023 can be downloaded at
807 <http://www.airqualitynju.com>

808 **Author contributions**

809 CGu developed the methodology, conducted the research and wrote the draft. YZhao
810 and LZhang developed the strategy and designed the research, and YZhao revised the
811 manuscript. YWang provided the support of machine learning modeling. YJi provided
812 the support of WFR-CMAQ. ZZhang, and WZhao supported emission data processing.
813 SSun, YBian, JZhu, and SZhong provided the support of emission data.



814 **Competing interests**

815 The authors declare that they have no conflict of interest.

816 **Acknowledgments**

817 This work was sponsored by the National Natural Science Foundation of China (grant
818 no. 42577116), the National Key Research and Development Program of China
819 (2023YFC3709802), the Key Research and Development Programme of Jiangsu
820 Province (BE2022838), and the Key Laboratory of Formation and Prevention of
821 Urban Air Pollution Complex, Ministry of Ecology and Environment (no.
822 2025080167).

823 **References**

824 An, J., Huang, Y., Huang, C., Wang, X., Yan, R., Wang, Q., Wang, H., Jing, S., Zhang,
825 Y., Liu, Y., Chen, Y., Xu, C., Qiao, L., Zhou, M., Zhu, S., Hu, Q., Lu, J., and
826 Chen, C.: Emission inventory of air pollutants and chemical speciation for
827 specific anthropogenic sources based on local measurements in the Yangtze
828 River Delta region, China, *Atmos. Chem. Phys.*, 21, 2003–2025,
829 <https://doi.org/10.5194/acp-21-2003-2021>, 2021.

830 BEIS: Provisional UK greenhouse gas emissions national statistics,
831 <https://www.gov.uk/government/statistics/> (last visited on October 2025), 2022.

832 Bo, X., Jia, M., Xue, X., Tang, L., Mi, Z., Wang, S., Cui, W., Chang, X., Ruan, J.,
833 Dong, G., Zhou, B., and Davis, S. J.: Effect of strengthened standards on Chinese
834 ironmaking and steelmaking emissions, *Nat. Sustain.*, 4, 811 - 820, 2021.

835 Carbon monitor: Global high spatial resolution near real time carbon map,
836 <https://www.carbonmonitor.org.cn/> (last visited on October 2025), 2024.

837 CBS: Emissions of greenhouse gases according to IPCC guidelines, quarter,
838 <https://www.cbs.nl/nl-nl/cijfers/detail/> (last visited on October 2025), 2024.

839 Chu, B., Ma, Q., Liu, J., Ma, J., Zhang, P., Chen, T., Feng, Q., Wang, C., Yang, N., Ma,



840 H., Ma, J., Russell, A. G., and He, H.: Air Pollutant Correlations in China:
841 Secondary Air Pollutant Responses to NO_x and SO₂ Control, Environ. Sci.
842 Technol. Lett., 7, 695–700, 10.1021/acs.estlett.0c00403, 2020.

843 CITEPA: Monthly emissions barometer, <https://www.citepa.org/fr/barometre/> (last
844 access: October 2025), 2024.

845 Cliff, S. J., Drysdale, W., Lee, J. D., Helfter, C., Nemitz, E., Metzger, S., and Barlow,
846 J. F.: Pandemic restrictions in 2020 highlight the significance of non-road NO_x
847 sources in central London, Atmos. Chem. Phys., 23, 2315–2330,
848 <https://doi.org/10.5194/acp-23-2315-2023>, 2023.

849 Crippa, M., Solazzo, E., Huang G., Guzzardi D., Koffi E., Muntean M., Schieberle C.,
850 Friedrich R.: High resolution temporal profiles in the Emissions Database for
851 Global Atmospheric Research, Sci. Data, 7, 121,
852 <https://doi.org/10.1038/s41597-020-0462-2>, 2020.

853 Department of Ecology and Environment of Jiangsu province (DEE).: Report on the
854 State of the Ecology and Environment in Jiangsu province, 2023.

855 Department of Ecology and Environment of Jiangsu province (DEE).: Emergency
856 Plan for Severe Air Pollution in Jiangsu Province, 2022.

857 Department of Industry and Information Technology of Jiangsu province (DII).:
858 Notice on Enterprises and Vehicles Intending to Apply for the 2022 Central
859 Government Subsidy Settlement Fund for the Promotion and Application of New
860 Energy Vehicles, 2023.

861 Ding, J., van der A, R. J., Mijling, B., Levelt, P. F., and Hao, N.: NO_x emission
862 estimates during the 2014 Youth Olympic Games in Nanjing, Atmos. Chem.
863 Phys., 15, 9399–9412, <https://doi.org/10.5194/acp-15-9399-2015>, 2015.

864 Dong, X., Zhang, Y., Yu, G., Xiong, Y., Han, Z., Huo, J., Huang, C., Kan, H., Zheng,
865 M., Ning, Z., and Xie, B.: Environmental and health impacts of reduced PM_{2.5}
866 and trace metals from ship emissions under low-sulfur fuel oil policy in Shanghai,
867 China, Environmental Pollution, 377, 126409,
868 <https://doi.org/10.1016/j.envpol.2025.126409>, 2025.

869 Dou, X., Wang, Y., Ciais, P., Chevallier, F., Davis, S. J., Crippa, M.,



870 Janssens-Maenhout, G., Guizzardi, D., Solazzo, E., Yan, F., Huo, D., Zheng, B.,
871 Zhu, B., Cui, D., Ke, P., Sun, T., Wang, H., Zhang, Q., Gentine, P., Deng, Z., and
872 Liu, Z.: Near-real-time global gridded daily CO₂ emissions, *The Innovation*, 3,
873 100182, <https://doi.org/10.1016/j.xinn.2021.100182>, 2022.

874 Emery, C., Liu, Z., Russell, A. G., Odman, M. T., Yarwood, G., and Kumar, N.:
875 Recommendations on statistics and benchmarks to assess photochemical model
876 performance, *J. Air Waste Manag. Assoc.*, 67, 582-598,
877 10.1080/10962247.2016.1265027, 2017.

878 Gaubert, B., Bouarar, I., Doumbia, T., Liu, Y., Stavrakou, T., Deroubaix, A., Darras, S.,
879 Elguindi, N., Granier, C., Lacey, F., Müller, J. F., Shi, X., Tilmes, S., Wang, T.,
880 and Brasseur, G. P.: Global changes in secondary atmospheric pollutants during
881 the 2020 COVID-19 pandemic, *J. Geophys. Res. Atmos.*, 126, e2020JD034213.
882 <https://doi.org/10.1029/2020JD034213>, 2021.

883 Geng, G., Xiao, Q., Liu, S., Liu, X., Cheng, J., Zheng, Y., Xue, T., Tong, D., Zheng, B.,
884 Peng, Y., Huang, X., He, K., and Zhang, Q.: Tracking Air Pollution in China:
885 Near Real-Time PM_{2.5} Retrievals from Multisource Data Fusion,
886 *Environ.Sci.Technol.*, 55, 12106-12115, 10.1021/acs.est.1c01863, 2021.

887 Geng, G., Liu, Y., Liu, Y., Liu, S., Cheng, J., Yan, L., Wu, N., Hu, H., Tong, D., Zheng,
888 B., Yin, Z., He, K., and Zhang, Q.: Efficacy of China's clean air actions to tackle
889 PM_{2.5} pollution between 2013 and 2020, *Nature Geoscience*, 17, 987–994,
890 10.1038/s41561-024-01540-z, 2024.

891 Gu, C., Zhang, L., Xu, Z., Xia, S., Wang, Y., Li, L., Wang, Z., Zhao, Q., Wang, H., and
892 Zhao, Y.: High-resolution regional emission inventory contributes to the
893 evaluation of policy effectiveness: a case study in Jiangsu Province, China,
894 *Atmos. Chem. Phys.*, 23, 4247–4269, <https://doi.org/10.5194/acp-23-4247-2023>,
895 2023.

896 Guevara, M., Jorba, O., Soret, A., Petetin, H., Bowdalo, D., Serradell, K., Tena, C.,
897 Denier van der Gon, H., Kuenen, J., Peuch, V.-H., and Pérez García-Pando, C.:
898 Time-resolved emission reductions for atmospheric chemistry modelling in
899 Europe during the COVID-19 lockdowns, *Atmos. Chem. Phys.*, 21, 773–797,



900 https://doi.org/10.5194/acp-21-773-2021, 2021.

901 Guevara, M., Petetin, H., Jorba, O., Denier van der Gon, H., Kuenen, J., Super, I.,
902 Granier, C., Doumbia, T., Ciais, P., Liu, Z., Lamboll, R. D., Schindlbacher, S.,
903 Matthews, B., and Pérez García-Pando, C.: Towards near-real-time air pollutant
904 and greenhouse gas emissions: lessons learned from multiple estimates during
905 the COVID-19 pandemic, *Atmos. Chem. Phys.*, 23, 8081–8101,
906 https://doi.org/10.5194/acp-23-8081-2023, 2023.

907 Harkins, C., McDonald, B. C., Henze, D. K., and Wiedinmyer, C.: A fuel-based
908 method for updating mobile source emissions during the COVID-19 pandemic,
909 *Environ. Res. Lett.*, 16, 065018, https://doi.org/10.1088/1748-9326/ac0660,
910 2021.

911 He K., Zhang Q., Wang S.: Technical manual for the preparation of urban air pollution
912 Source emission inventory, China Statistics Press, Beijing, 2018 (in Chinese).

913 Hu, W., Zhao, Y., Lu, N., Wang, X., Zheng, B., Henze, D. K., Zhang, L., Fu, T.-M.,
914 and Zhai, S.: Changing Responses of PM_{2.5} and Ozone to Source Emissions in
915 the Yangtze River Delta Using the Adjoint Model, *Environ. Sci. Technol.*, 58,
916 628-638, 10.1021/acs.est.3c05049, 2024.

917 Huang, C., An, J., Wang, H., Liu, Q., Tian, J., Wang, Q., Hu, Q., Yan, R., Shen, Y.,
918 Duan, Y., Fu, Q., Shen, J., Ye, H., Wang, M., Wei, C., Cheng, Y., and Su, H.:
919 Highly Resolved Dynamic Emissions of Air Pollutants and Greenhouse Gas CO₂
920 during COVID-19 Pandemic in East China, *Environ.Sci.Technol.Lett.*, 8,
921 853-860, 10.1021/acs.estlett.1c00600, 2021.

922 Huo, D., Huang, X., Dou, X., Ciais, P., Li, Y., Deng, Z., Wang, Y., Cui, D., Benkhelifa,
923 F., Sun, T., Zhu, B., Roest, G., Gurney, K. R., Ke, P., Guo, R., Lu, C., Lin, X.,
924 Lovell, A., Appleby, K., DeCola, P. L., Davis, S. J., and Liu, Z.: Carbon Monitor
925 Cities near-real-time daily estimates of CO₂ emissions from 1500 cities
926 worldwide, *Sci. Data*, 9, 533, 10.1038/s41597-022-01657-z, 2022.

927 Kholod, N., Evans, M., Gusev, E., Yu, S., Malyshev, V., and Barinov, A.: A
928 methodology for calculating transport emissions in cities with limited traffic data:
929 Case study of diesel particulates and black carbon emissions in Murmansk, *Sci.*



930 Total Environ., 547, 305-313, <https://doi.org/10.1016/j.scitotenv.2015.12.151>,
931 2016.

932 Kurokawa, J. and Ohara, T.: Long-term historical trends in air pollutant emissions in
933 Asia: Regional Emission inventory in ASia (REAS) version 3, Atmos. Chem.
934 Phys., 20, 12761–12793, <https://doi.org/10.5194/acp-20-12761-2020>, 2020.

935 Lei, T., Wang, D., Yu, X., Ma, S., Zhao, W., Cui, C., Meng, J., Tao, S., and Guan, D.:
936 Global iron and steel plant CO₂ emissions and carbon-neutrality pathways,
937 Nature, 622, 514–520, 10.1038/s41586-023-06486-7, 2023.

938 Li, K., Jacob, D. J., Shen, L., Lu, X., De Smedt, I., and Liao, H.: Increases in surface
939 ozone pollution in China from 2013 to 2019: anthropogenic and meteorological
940 influences, Atmos. Chem. Phys., 20, 11423–11433,
941 <https://doi.org/10.5194/acp-20-11423-2020>, 2020.

942 Li, K., Jacob, D. J., Liao, H., Qiu, Y., Shen, L., Zhai, S., Bates, K. H., Sulprizio, M. P.,
943 Song, S., Lu, X., Zhang, Q., Zheng, B., Zhang, Y., Zhang, J., Lee, H. C., and Kuk,
944 S. K.: Ozone pollution in the North China Plain spreading into the late-winter
945 haze season, Proc. Natl. Acad. Sci., 118, e2015797118,
946 doi:10.1073/pnas.2015797118, 2021.

947 Li, M., Zhang, Q., Zheng, B., Tong, D., Lei, Y., Liu, F., Hong, C., Kang, S., Yan, L.,
948 Zhang, Y., Bo, Y., Su, H., Cheng, Y., and He, K.: Persistent growth of
949 anthropogenic non-methane volatile organic compound (NMVOC) emissions in
950 China during 1990–2017: drivers, speciation and ozone formation potential,
951 Atmos. Chem. Phys., 19, 8897–8913, <https://doi.org/10.5194/acp-19-8897-2019>,
952 2019.

953 Li, H. and Zheng, B.: TROPOMI NO₂ Shows a Fast Recovery of China's Economy in
954 the First Quarter of 2023, Environ. Sci. Technol. Lett., 10, 635-641,
955 10.1021/acs.estlett.3c00386, 2023.

956 Liu, F., Page, A., Strode, S. A., Yoshida, Y., Choi, S., Zheng, B., Lamsal, L. N., Li, C.,
957 Krotkov, N. A., Eskes, H., van der A, R., Veefkind, P., Levelt, P. F., Hauser, O. P.,
958 and Joiner, J.: Abrupt decline in tropospheric nitrogen dioxide over China after
959 the outbreak of COVID-19, Sci. Adv., 6, eabc2992,



960 https://doi.org/10.1126/sciadv.abc2992, 2020.

961 Liu, M., Shang, F., Lu, X., Huang, X., Song, Y., Liu, B., Zhang, Q., Liu, X., Cao, J.,
962 Xu, T., Wang, T., Xu, Z., Xu, W., Liao, W., Kang, L., Cai, X., Zhang, H., Dai, Y.,
963 and Zhu, T.: Unexpected response of nitrogen deposition to nitrogen oxide
964 controls and implications for land carbon sink, *Nat. Commun.*, 13, 3126,
965 10.1038/s41467-022-30854-y, 2022.

966 Liu, X., Yang, L., Du, J., Zhang, H., Hu, J., Chen, A., and Lv, W.: Carbon and air
967 pollutant emissions forecast of China's cement industry from 2021 to 2035,
968 Resources, Conservation and Recycling, 204, 107498,
969 https://doi.org/10.1016/j.resconrec.2024.107498, 2024.

970 Liu, Z., Ciais, P., Deng, Z., Davis, S. J., Zheng, B., Wang, Y., Cui, D., Zhu, B., Dou,
971 X., Ke, P., Sun, T., Guo, R., Zhong, H., Boucher, O., Bréon, F.-M., Lu, C., Guo,
972 R., Xue, J., Boucher, E., Tanaka, K., and Chevallier, F.: Carbon Monitor, a
973 near-real-time daily dataset of global CO₂ emission from fossil fuel and cement
974 production, *Sci. Data*, 7, 392, https://doi.org/10.1038/s41597-020-00708-7,
975 2020a.

976 Liu, Z., Ciais, P., Deng, Z., Lei, R., Davis, S. J., Feng, S., Zheng, B., Cui, D., Dou, X.,
977 Zhu, B., Guo, R., Ke, P., Sun, T., Lu, C., He, P., Wang, Y., Yue, X., Wang, Y., Lei,
978 Y., Zhou, H., Cai, Z., Wu, Y., Guo, R., Han, T., Xue, J., Boucher, O., Boucher, E.,
979 Chevallier, F., Tanaka, K., Wei, Y., Zhong, H., Kang, C., Zhang, N., Chen, B., Xi,
980 F., Liu, M., Bréon, F.-M., Lu, Y., Zhang, Q., Guan, D., Gong, P., Kammen, D. M.,
981 He, K., and Schellnhuber, H. J.: Near-real-time monitoring of global CO₂
982 emissions reveals the effects of the COVID-19 pandemic, *Nat. Commun.*, 11,
983 5172, https://doi.org/10.1038/s41467-020-18922-7, 2020b.

984 Lv, Z., Wang, X., Deng, F., Ying, Q., Archibald, A. T., Jones, R. L., Ding, Y., Cheng,
985 Y., Fu, M., Liu, Y., Man, H., Xue, Z., He, K., Hao, J., and Liu, H.: Source–
986 Receptor Relationship Revealed by the Halted Traffic and Aggravated Haze in
987 Beijing during the COVID-19 Lockdown, *Environ. Sci. Technol.*, 54,
988 15660–15670, 10.1021/acs.est.0c04941, 2020.

989 Ma, Q., Wang, J., Xiong, M., and Zhu, L.: Air Quality Index (AQI) Did Not Improve



990 during the COVID-19 Lockdown in Shanghai, China, in 2022, Based on Ground
991 and TROPOMI Observations, *Remote Sens.*, 15, 1295, 2023.

992 Ministry of ecology and environment (MEE).: The list of technical specifications for
993 the application and issuance of pollutant discharge permits issued by the ministry
994 of ecology and environment, 2021.

995 Ministry of ecology and environment (MEE).: Report on the State of the Ecology and
996 Environment in China, 2022.

997 MEIC: Multi-resolution Emission Inventory model for Climate and air pollution
998 research, <http://meicmodel.org.cn/> (last visited on October 2025), 2024.

999 National Bureau of Statistics of China (NBS): Statistical Yearbook of China, China
1000 Statistics Press, Beijing, 2023 (in Chinese).

1001 Requia, W. J., Di, Q., Silvern, R., Kelly, J. T., Koutrakis, P., Mickley, L. J., Sulprizio,
1002 M. P., Amini, H., Shi, L., and Schwartz, J.: An Ensemble Learning Approach for
1003 Estimating High Spatiotemporal Resolution of Ground-Level Ozone in the
1004 Contiguous United States, *Environ. Sci. Technol.*, 54, 11037-11047,
1005 10.1021/acs.est.0c01791, 2020.

1006 State Council of the People's Republic of China. Three-year Action Plan for
1007 Protecting Blue Sky. Central Government of the People's Republic of China
1008 (2018). http://www.gov.cn/zhengce/content/2018-07/03/content_5303158.htm.

1009 Schneider, R., Masselot, P., Vicedo-Cabrera, A. M., Sera, F., Blangiardo, M., Forlani,
1010 C., Douros, J., Jorba, O., Adani, M., Kouznetsov, R., Couvidat, F., Arteta, J.,
1011 Raux, B., Guevara, M., Colette, A., Barré, J., Peuch, V.-H., and Gasparini, A.:
1012 Differential impact of government lockdown policies on reducing air pollution
1013 levels and related mortality in Europe, *Sci. Rep.*, 12, 726,
1014 <https://doi.org/10.1038/s41598-021-04277-6>, 2022.

1015 Shao, Y., Liu, R., Yang, J., Liu, M., Fang, W., Hu, L., Bi, J., and Ma, Z.: Economic
1016 Growth Facilitates Household Fuel Use Transition to Reduce PM_{2.5}-Related
1017 Deaths in China, *Environ. Sci. Technol.*, 57, 12663-12673,
1018 10.1021/acs.est.3c03276, 2023.

1019 Shen, X., Kong, L., Shi, Y., Cao, X., Li, X., Wu, B., Zhang, H., and Yao, Z.:
36



1020 Multi-type Air Pollutant Emission Inventory of Non-road Mobile Sources in
1021 China for the Period 1990-2017, *Aerosol Air Qual. Res.*, 21, 210003,
1022 10.4209/aaqr.210003, 2021.

1023 Shen, X., Che, H., Lv, T., Wu, B., Cao, X., Li, X., Zhang, H., Hao, X., Zhou, Q., and
1024 Yao, Z.: Real-world emission characteristics of
1025 semivolatile/intermediate-volatility organic compounds originating from nonroad
1026 construction machinery in the working process, *Sci. Total Environ.*, 858, 159970,
1027 <https://doi.org/10.1016/j.scitotenv.2022.159970>, 2023.

1028 Simayi, M., Shi, Y., Xi, Z., Ren, J., and Xie, S.: Emission trends of industrial VOCs in
1029 China since the clean air action and future reduction perspectives, *Sci. Total
1030 Environ.*, 826, 153994, <https://doi.org/10.1016/j.scitotenv.2022.153994>, 2022.

1031 Sokhi, R. S., Moussiopoulos, N., Baklanov, A., Bartzis, J., Coll, I., Finardi, S.,
1032 Friedrich, R., Geels, C., Grönholm, T., Halenka, T., Ketzel, M., Maragkidou, A.,
1033 Matthias, V., Moldanova, J., Ntziachristos, L., Schäfer, K., Suppan, P., Tsegas, G.,
1034 Carmichael, G., Franco, V., Hanna, S., Jalkanen, J.-P., Velders, G. J. M., and
1035 Kukkonen, J.: Advances in air quality research – current and emerging
1036 challenges, *Atmos. Chem. Phys.*, 22, 4615–4703,
1037 <https://doi.org/10.5194/acp-22-4615-2022>, 2022.

1038 Sun, S., Jin, J., Xia, M., Liu, Y., Gao, M., Zou, C., Wang, T., Lin, Y., Wu, L., Mao, H.,
1039 and Wang, P.: Vehicle emissions in a middle-sized city of China: Current status
1040 and future trends, *Environ. Int.*, 137, 105514,
1041 <https://doi.org/10.1016/j.envint.2020.105514>, 2020.

1042 State Council of the People's Republic of China. Three-year Action Plan for
1043 Protecting Blue Sky. Central People's Government of the People's Republic of
1044 China
1045 http://www.gov.cn/zhengce/content/2018-07/03/content_5303158.htm.

1046 Tang, L., Qu, J., Mi, Z., Bo, X., Chang, X., Anadon, L. D., Wang, S., Xue, X., Li, S.,
1047 Wang, X., and Zhao, X.: Substantial emission reductions from Chinese power
1048 plants after the introduction of ultra-low emissions standards, *Nat. Energy*, 4,
1049 929-938, 10.1038/s41560-019-0468-1, 2019.



1050 Tang, L., Ruan, J., Bo, X., Mi, Z., Wang, S., Dong, G., and Davis, S. J.: Plant-level
1051 real-time monitoring data reveal substantial abatement potential of air pollution
1052 and CO₂ in China's cement sector, *One Earth*, 5, 892-906,
1053 <https://doi.org/10.1016/j.oneear.2022.07.003>, 2022.

1054 Tong, D., Geng, G., Zhang, Q., Cheng, J., Qin, X., Hong, C., He, K., and Davis, S. J.:
1055 Health co-benefits of climate change mitigation depend on strategic power plant
1056 retirements and pollution controls, *Nat. Clim. Chang.*, 11, 1077-1083,
1057 [10.1038/s41558-021-01216-1](https://doi.org/10.1038/s41558-021-01216-1), 2021.

1058 Wang, F., Li, Z., Zhang, K., Di, B., and Hu, B.: An overview of non-road equipment
1059 emissions in China, *Atmos. Environ.*, 132, 283-289,
1060 <https://doi.org/10.1016/j.atmosenv.2016.02.046>, 2016.

1061 Wang, H., He, Q., Kong, H., Qin, K., Zheng, B., Lin, J., and Zhao, Y.: Declining
1062 short-term emission control opportunity for major events in Chinese cities,
1063 *Nature Cities*, 2, 434–446, [10.1038/s44284-025-00233-x](https://doi.org/10.1038/s44284-025-00233-x), 2025.

1064 Wang, K., Gao, J., Tian, H., Dan, M., Yue, T., Xue, Y., Zou, P., and Wang, C.: An
1065 emission inventory spatial allocate method based on POI data, *China
1066 Environmental Science*, 37, 2377-2382, 2017.

1067 Wang, N., Xu, J., Pei, C., Tang, R., Zhou, D., Chen, Y., Li, M., Deng, X., Deng, T.,
1068 Huang, X., and Ding, A.: Air quality during COVID-19 lockdown in the Yangtze
1069 River Delta and the Pearl River Delta: Two different responsive mechanisms to
1070 emission reductions in China, *Environ. Sci. Technol.*, 55, 5721-5730,
1071 [10.1021/acs.est.0c08383](https://doi.org/10.1021/acs.est.0c08383), 2021.

1072 Wang, S. W., Zhang, Q., Streets, D. G., He, K. B., Martin, R. V., Lamsal, L. N., Chen,
1073 D., Lei, Y., and Lu, Z.: Growth in NO_x emissions from power plants in China:
1074 bottom-up estimates and satellite observations, *Atmos. Chem. Phys.*, 12, 4429–
1075 4447, [doi:10.5194/acp-12-4429-2012](https://doi.org/10.5194/acp-12-4429-2012), 2012.

1076 Wang, L., Liu, D., Yan, W., Kang, Z., Liu, R., Zhang, J., and Li, Z.: Spatio-temporal
1077 distribution, transport characteristics and synoptic patterns of ozone pollution
1078 near surface in Jiangsu province, China, *Atmos. Pollut. Res.*, 13, 101616,
1079 <https://doi.org/10.1016/j.apr.2022.101616>, 2022.



1080 Wang, Y., Zhao, Y., Liu, Y., Jiang, Y., Zheng, B., Xing, J., Liu, Y., Wang, S., and
1081 Nielsen, C. P.: Sustained emission reductions have restrained the ozone pollution
1082 over China, *Nat. Geosci.*, 16, 967-974, 10.1038/s41561-023-01284-2, 2023.

1083 Xiao, Q., Chang, H. H., Geng, G., and Liu, Y.: An Ensemble Machine-Learning
1084 Model To Predict Historical PM_{2.5} Concentrations in China from Satellite Data,
1085 *Environ. Sci. Tech.*, 52, 13260-13269, 10.1021/acs.est.8b02917, 2018.

1086 Xu, Y., Chen, S., Wang, Z., Liu, B., and Wang, L.: Multi-Scale Dynamics and Spatial
1087 Consistency of Economy and Population Based on NPP/VIIRS Nighttime Light
1088 Data and Population Imagery: A Case Study of the Yangtze River Delta, *Remote
1089 Sens.*, 16, 2806, 2024.

1090 Xu, R., Tong, D., Xiao, Q., Qin, X., Chen, C., Yan, L., Cheng, J., Cui, C., Hu, H., Liu,
1091 W., Yan, X., Wang, H., Liu, X., Geng, G., Lei, Y., Guan, D., He, K., and Zhang,
1092 Q. MEIC-global-CO₂: A new global CO₂ emission inventory with
1093 highly-resolved source category and sub-country information, *Sci. China Earth
1094 Sci.*, 66, doi: 10.1007/s11430-023-1230-3, 2023.

1095 Yang, X. F., Liu, H., Man, H. Y., and He, K. B.: Characterization of road freight
1096 transportation and its impact on the national emission inventory in China, *Atmos.
1097 Chem. Phys.*, 15, 2105–2118, <https://doi.org/10.5194/acp-15-2105-2015>, 2015.

1098 Yang, D., Zhang, S., Niu, T., Wang, Y., Xu, H., Zhang, K. M., and Wu, Y.:
1099 High-resolution mapping of vehicle emissions of atmospheric pollutants based
1100 on large-scale, real-world traffic datasets, *Atmos. Chem. Phys.*, 19, 8831–8843,
1101 <https://doi.org/10.5194/acp-19-8831-2019>, 2019.

1102 Yang, L., Hu, Y.-J., Wang, H., Li, C., Tang, B.-J., Wang, B., and Cui, H.: Uncertainty
1103 quantification of CO₂ emissions from China's civil aviation industry to 2050,
1104 *J. Environ. Manage.*, 336, 117624,
1105 <https://doi.org/10.1016/j.jenvman.2023.117624>, 2023.

1106 Yun, X., Meng, W., Xu, H., Zhang, W., Yu, X., Shen, H., Chen, Y., Shen, G., Ma, J., Li,
1107 B., Cheng, H., Hu, J., and Tao, S.: Coal Is Dirty, but Where It Is Burned
1108 Especially Matters, *Environ. Sci. Tech.*, 55, 7316-7326, 10.1021/acs.est.1c01148,
1109 2021.



1110 Zhan, Y., Xie, M., Zhao, W., Wang, T., Gao, D., Chen, P., Tian, J., Zhu, K., Li, S.,
1111 Zhuang, B., Li, M., Luo, Y., and Zhao, R.: Quantifying the seasonal variations in
1112 and regional transport of PM_{2.5} in the Yangtze River Delta region, China:
1113 characteristics, sources, and health risks, *Atmos. Chem. Phys.*, 23, 9837–9852,
1114 <https://doi.org/10.5194/acp-23-9837-2023>, 2023.

1115 Zhang, B., Zhang, J., and Feng, T.: A global comparative study on the impact of
1116 COVID-19 policy on atmospheric nitrogen dioxide (NO₂): Evidence from remote
1117 sensing data in 2019–2022, *J. Environ. Manage.*, 367, 121851,
1118 <https://doi.org/10.1016/j.jenvman.2024.121851>, 2024.

1119 Zhang, Q., Zheng, Y., Tong, D., Shao, M., Wang, S., Zhang, Y., Xu, X., Wang, J., He,
1120 H., Liu, W., Ding, Y., Lei, Y., Li, J., Wang, Z., Zhang, X., Wang, Y., Cheng, J.,
1121 Liu, Y., Shi, Q., Yan, L., Geng, G., Hong, C., Li, M., Liu, F., Zheng, B., Cao, J.,
1122 Ding, A., Gao, J., Fu, Q., Huo, J., Liu, B., Liu, Z., Yang, F., He, K., and Hao, J.:
1123 Drivers of improved PM_{2.5} air quality in China from 2013 to 2017, *Proc. Natl.
1124 Acad. Sci.*, 116, 24463–24469, doi:10.1073/pnas.1907956116, 2019.

1125 Zhang, S., Zhang, C., Cai, W., Bai, Y., Callaghan, M., Chang, N., Chen, B., Chen, H.,
1126 Cheng, L., Dai, H., Dai, X., Fan, W., Fang, X., Gao, T., Geng, Y., Guan, D., Hu,
1127 Y., Hua, J., Huang, C., Huang, H., Huang, J., Huang, X., Ji, J. S., Jiang, Q., Jiang,
1128 X., Kiesewetter, G., Li, T., Liang, L., Lin, B., Lin, H., Liu, H., Liu, Q., Liu, X.,
1129 Liu, Z., Liu, Z., Liu, Y., Lu, B., Lu, C., Luo, Z., Ma, W., Mi, Z., Ren, C.,
1130 Romanello, M., Shen, J., Su, J., Sun, Y., Sun, X., Tang, X., Walawender, M.,
1131 Wang, C., Wang, Q., Wang, R., Warnecke, L., Wei, W., Wen, S., Xie, Y., Xiong,
1132 H., Xu, B., Yan, Y., Yang, X., Yao, F., Yu, L., Yuan, J., Zeng, Y., Zhang, J., Zhang,
1133 L., Zhang, R., Zhang, S., Zhang, S., Zhao, M., Zheng, D., Zhou, H., Zhou, J.,
1134 Zhou, Z., Luo, Y., and Gong, P.: The 2023 China report of the Lancet Countdown
1135 on health and climate change: taking stock for a thriving future, *The Lancet
1136 Public Health*, 8, e978–e995, 10.1016/S2468-2667(23)00245-1, 2023.

1137 Zhang, Y., Yang, X., Brown, R., Yang, L., Morawska, L., Ristovski, Z., Fu, Q., and
1138 Huang, C.: Shipping emissions and their impacts on air quality in China, *Sci.
1139 Total Environ.*, 581, 186–198, <https://doi.org/10.1016/j.scitotenv.2016.12.098>,



1140 2017.

1141 Zhang, Y., Bo, X., Zhao, Y., and Nielsen, C. P.: Benefits of current and future policies
1142 on emissions of China's coal-fired power sector indicated by continuous emission
1143 monitoring, Environ. Pollut., 251, 415-424,
1144 <https://doi.org/10.1016/j.envpol.2019.05.021>, 2019.

1145 Zhao, Y., Wang, S., Nielsen, C. P., Li, X., and Hao, J.: Establishment of a database of
1146 emission factors for atmospheric pollutants from Chinese coal-fired power plants,
1147 Atmos. Environ., 44, 1515-1523, <https://doi.org/10.1016/j.atmosenv.2010.01.017>,
1148 2010.

1149 Zhao, Y., Zhang, J., and Nielsen, C. P.: The effects of recent control policies on trends
1150 in emissions of anthropogenic atmospheric pollutants and CO₂ in China, Atmos.
1151 Chem. Phys., 13, 487-508, 10.5194/acp-13-487-2013, 2013.

1152 Zhao, Y., Zhang, K., Xu, X., Shen, H., Zhu, X., Zhang, Y., Hu, Y., and Shen, G.:
1153 Substantial Changes in Nitrogen Dioxide and Ozone after Excluding
1154 Meteorological Impacts during the COVID-19 Outbreak in Mainland China,
1155 Environ. Sci. Tech. Lett., 7, 402–408, <https://doi.org/10.1021/acs.estlett.0c00304>,
1156 2020a.

1157 Zhao, Y., Yuan, M., Huang, X., Chen, F., and Zhang, J.: Quantification and evaluation
1158 of atmospheric ammonia emissions with different methods: a case study for the
1159 Yangtze River Delta region, China, Atmos. Chem. Phys., 20, 4275–4294,
1160 <https://doi.org/10.5194/acp-20-4275-2020>, 2020b.

1161 Zhao, Y., Xi, M., Zhang, Q., Dong, Z., Ma, M., Zhou, K., Xu, W., Xing, J., Zheng, B.,
1162 Wen, Z., Liu, X., Nielsen, C. P., Liu, Y., Pan, Y., and Zhang, L.: Decline in bulk
1163 deposition of air pollutants in China lags behind reductions in emissions, Nat.
1164 Geosci., 15, 190–195, <https://doi.org/10.1038/s41561-022-00899-1>, 2022.

1165 Zhao, X., Shao, B., Su, J., and Tian, N.: Exploring synergistic evolution of carbon
1166 emissions and air pollutants and spatiotemporal heterogeneity of influencing
1167 factors in Chinese cities, Sci. Rep., 15, 2657, 10.1038/s41598-024-84212-7,
1168 2025.

1169 Zheng, B., Tong, D., Li, M., Liu, F., Hong, C., Geng, G., Li, H., Li, X., Peng, L., Qi, J.,



1170 Yan, L., Zhang, Y., Zhao, H., Zheng, Y., He, K., and Zhang, Q.: Trends in China's
1171 anthropogenic emissions since 2010 as the consequence of clean air actions,
1172 *Atmos. Chem. Phys.*, 18, 14095–14111,
1173 <https://doi.org/10.5194/acp-18-14095-2018>, 2018.

1174 Zheng, B., G. Geng, P. Ciais, S. J. Davis, R. V. Martin, J. Meng, N. Wu, F. Chevallier,
1175 G. Broquet, F. Boersma, R. J. van der A, J. Lin, D. Guan, Y. Lei, K. He, Q.
1176 Zhang. Satellite-based estimates of decline and rebound in China's CO₂
1177 emissions during COVID-19 pandemic. *Sci. Adv.*, 6, eabd4998, 2020.

1178 Zheng, B., Zhang, Q., Geng, G., Chen, C., Shi, Q., Cui, M., Lei, Y., and He, K.:
1179 Changes in China's anthropogenic emissions and air quality during the
1180 COVID-19 pandemic in 2020, *Earth Syst. Sci. Data*, 13, 2895–2907,
1181 <https://doi.org/10.5194/essd-13-2895-2021>, 2021.

1182 Zhou, Y., Zhao, Y., Mao, P., Zhang, Q., Zhang, J., Qiu, L., and Yang, Y.: Development
1183 of a high-resolution emission inventory and its evaluation and application
1184 through air quality modeling for Jiangsu Province, China, *Atmos. Chem. Phys.*,
1185 17, 211–233, <https://doi.org/10.5194/acp-17-211-2017>, 2017.

1186 Zhou, Z., Tan, Q., Liu, H., Deng, Y., Wu, K., Lu, C., and Zhou, X.: Emission
1187 characteristics and high-resolution spatial and temporal distribution of pollutants
1188 from motor vehicles in Chengdu, China, *Atmos. Pollut. Res.*, 10, 749–758,
1189 <https://doi.org/10.1016/j.apr.2018.12.002>, 2019.

1190 Zhou, K., Xu, W., Zhang, L., Ma, M., Liu, X., and Zhao, Y.: Estimating nitrogen and
1191 sulfur deposition across China during 2005 to 2020 based on multiple statistical
1192 models, *Atmos. Chem. Phys.*, 23, 8531–8551,
1193 <https://doi.org/10.5194/acp-23-8531-2023>, 2023.

1194



1195 **Figure captions**

1196 **Figure 1** The research framework of near-real-time emission estimation and
1197 application in this work.

1198 **Figure 2** Daily emission estimates of anthropogenic air pollutants by sector for
1199 Jiangsu Province in 2022. (a) NO_x; (b) SO₂; (c) PM_{2.5}; (d) NMVOCs; (e) NH₃.

1200 **Figure 3** Spatial distribution of anthropogenic NO_x emissions for Jiangsu Province in
1201 2022 with a horizontal resolution of 3×3 km. (a) Total emissions; (b) Power; (c)
1202 Industry; (d) Vehicle; (e) Off-road transportation; (f) Residential. The map data
1203 provided by Resource and Environment Data Cloud Platform are freely available for
1204 academic use (<http://www.resdc.cn/data.aspx?DATAID=201>), © Institute of
1205 Geographic Sciences & Natural Resources Research, Chinese Academy of Sciences.

1206 **Figure 4** The monthly air pollutant emissions for Jiangsu Province in 2022 estimated
1207 in this study (a, c, and e) and in national emission inventory (MEIC; b, d, and f). The
1208 emissions of SO₂ (a and b), NO_x (c and d) and primary PM_{2.5} (e and f) are contained.
1209 The red lines with triangles represent the observed monthly surface concentrations of
1210 corresponding air pollutants.

1211 **Figure 5** The differences between the emissions of NO_x (a), SO₂ (b), PM_{2.5} (c) and
1212 NMVOCs (d) in April-May for 2022 and 2023 in Jiangsu Province. The first column
1213 illustrates the daily total emissions and the differences for the period of the two years.
1214 The second column illustrates the contributions of various source categories to the
1215 differences in daily total emissions, and the third column aggregates them for the
1216 whole period.

1217 **Figure 6** The comparison between the observed daily PM_{2.5} concentrations and those
1218 simulated with different emission inventories (this work and MEIC) for January, April,
1219 July and October 2022 for Jiangsu Province.

1220 **Figure 7** The comparison between the observed daily O₃ concentrations and those
1221 simulated with different emission inventories (this work and MEIC) for January, April,



1222 July and October 2022 for Jiangsu Province.

1223 **Figure 8** The monthly anomaly in PM_{2.5} (a) and MDA8 O₃ concentrations (b) driven
1224 by the changing daily emissions for Jiangsu Province in 2022, based on the MLR
1225 model.

1226 **Figure 9** Anthropogenic pollutant and sector drivers of PM_{2.5} and MDA8 O₃
1227 variability. (a) and (b) illustrate the contributions of pollutant-sector combinations to
1228 the variability of PM_{2.5} in January and that of O₃ in July, derived from SHAP analysis.
1229 The black dashed lines represent the observed daily ground-level concentrations of
1230 PM_{2.5} and MDA8 O₃. (c) and (d) provided the contributions of the changing emissions
1231 from different sectors, with those of various precursor species aggregated.



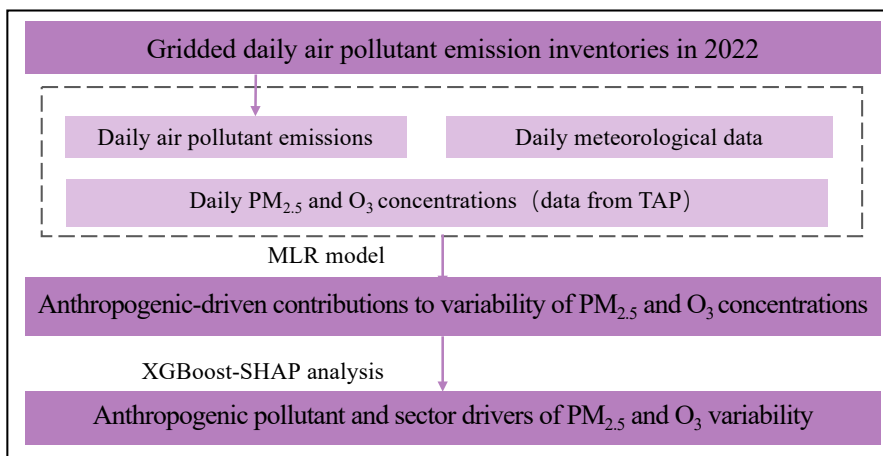
Basic data collection and processing

Enterprise data extraction		Raster data update (3km×3km)	
Location/Energy/Production		Road network	Waterway network
Manufacturing technology		Population	Land use types
Treatment process		GDP	Building footprint

Near-real-time activity data of multiple sources

Power/Industry	CEMS data	Electricity load
Vehicles	Congestion index	Traffic volume
Off-road	Construction data	Marine traffic
	Meteorological data	Flightradar24
Residential	PMI data	Farming work
Agricultural	PMI data	Freight volume
		HDD18
		Meteorological data

Construction and application of near real-time emissions



1232

1233 **Figure 1** The research framework of near-real-time emission estimation and
1234 application in this work.

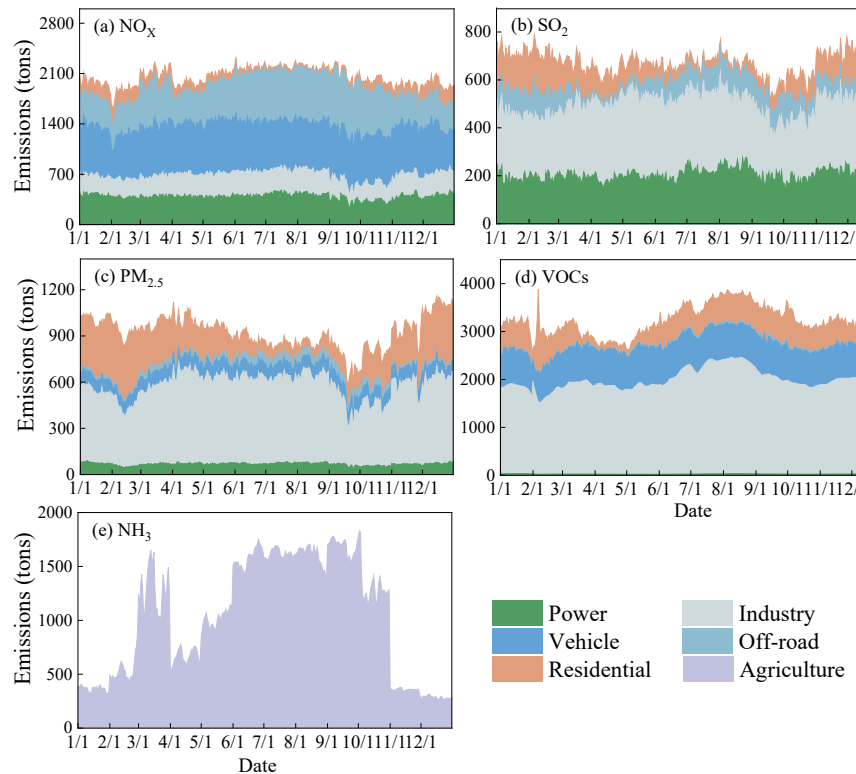


Figure 2 Daily emission estimates of anthropogenic air pollutants by sector for Jiangsu Province in 2022. (a) NO_x ; (b) SO_2 ; (c) $\text{PM}_{2.5}$; (d) NMVOCs; (e) NH_3 .

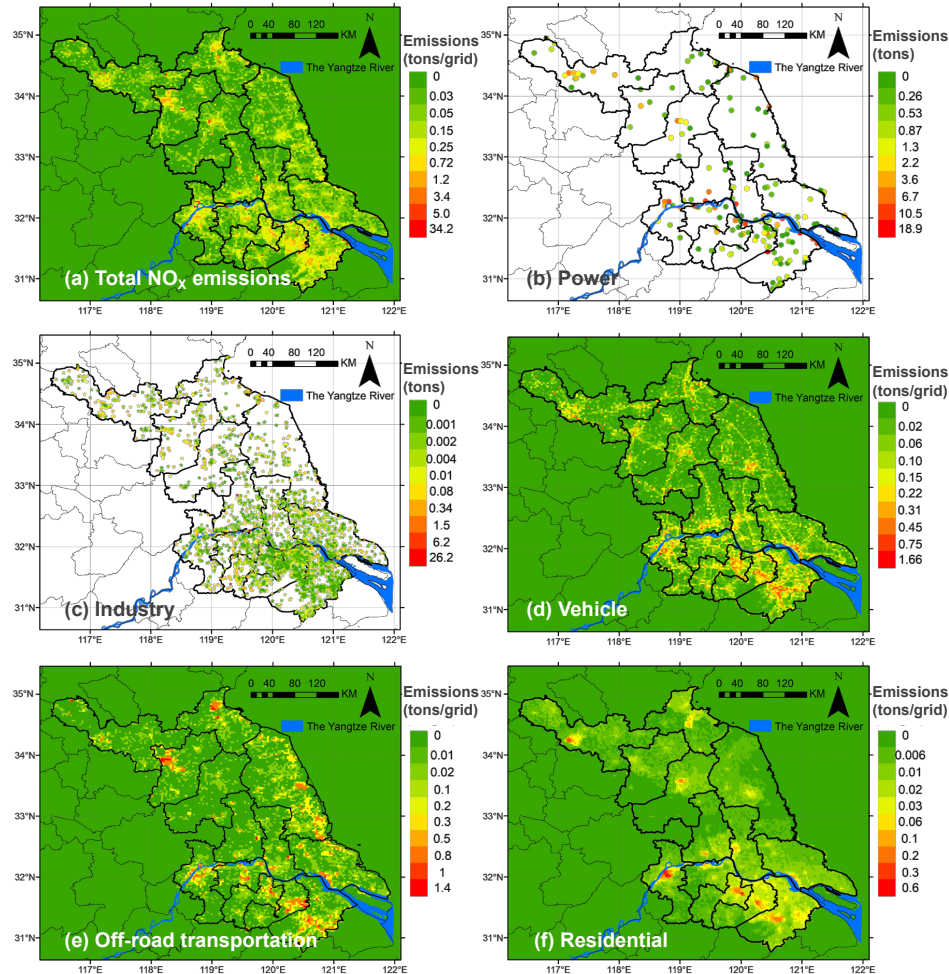


Figure 3 Spatial distribution of anthropogenic NO_x emissions for Jiangsu Province in 2022 with a horizontal resolution of 3×3 km. (a) Total emissions; (b) Power; (c) Industry; (d) Vehicle; (e) Off-road transportation; (f) Residential. The map data provided by Resource and Environment Data Cloud Platform are freely available for academic use (<http://www.resdc.cn/data.aspx?DATAID=201>), © Institute of Geographic Sciences & Natural Resources Research, Chinese Academy of Sciences.

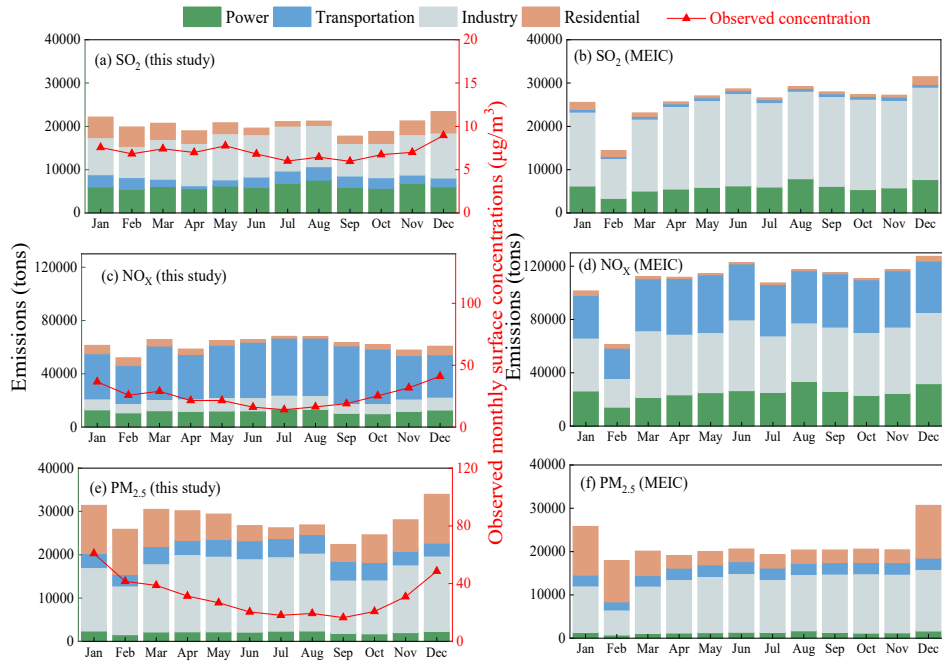


Figure 4 The monthly air pollutant emissions for Jiangsu Province in 2022 estimated in this study (a, c, and e) and in national emission inventory (MEIC; b, d, and f). The emissions of SO_2 (a and b), NO_x (c and d) and primary $\text{PM}_{2.5}$ (e and f) are contained. The red lines with triangles represent the observed monthly surface concentrations of corresponding air pollutants.

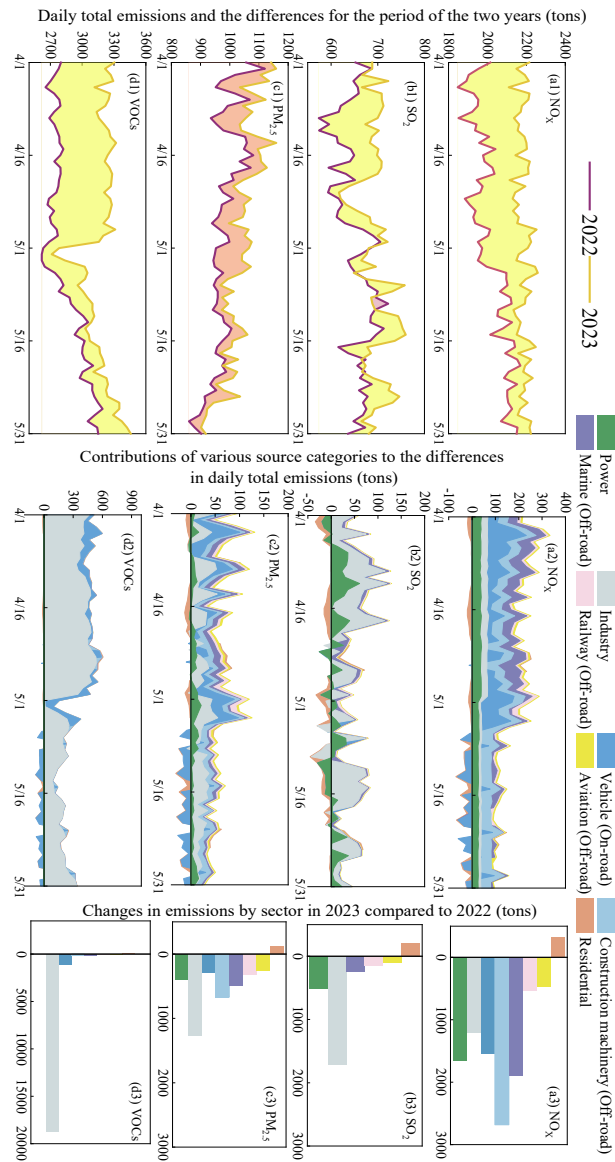


Figure 5 The differences between the emissions of NO_x (a), SO₂ (b), PM_{2.5} (c) and NMVOCs (d) in April-May for 2022 and 2023 in Jiangsu Province. The first column illustrates the daily total emissions and the differences for the period of the two years. The second column illustrates the contributions of various source categories to the differences in daily total emissions, and the third column aggregates them for the whole period.

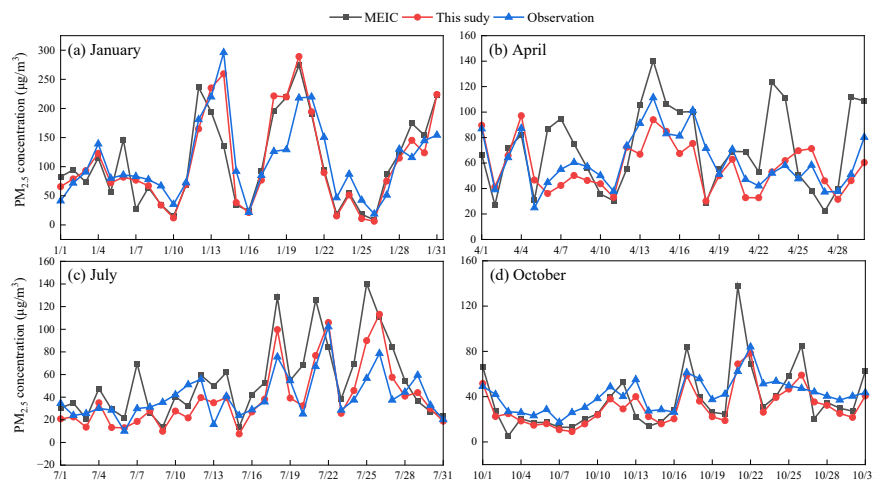


Figure 6 The comparison between the observed daily PM_{2.5} concentrations and those simulated with different emission inventories (this work and MEIC) for January, April, July and October 2022 for Jiangsu Province.

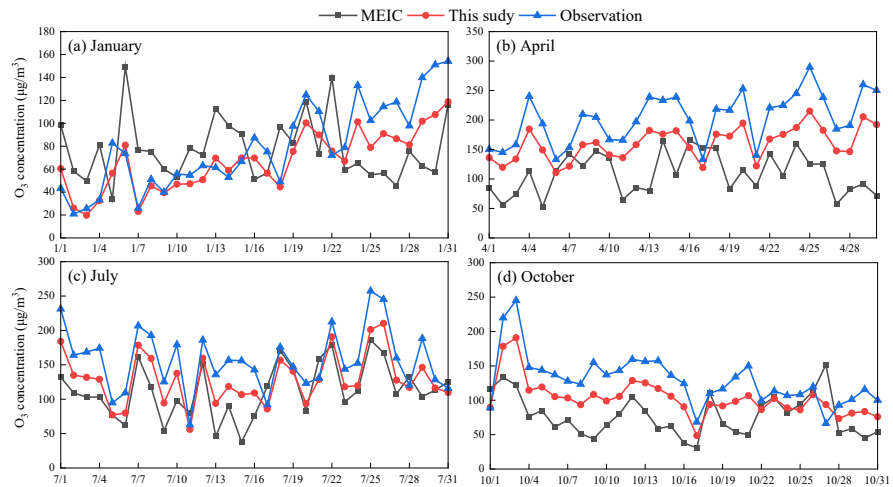


Figure 7 The comparison between the observed daily O₃ concentrations and those simulated with different emission inventories (this work and MEIC) for January, April, July and October 2022 for Jiangsu Province.

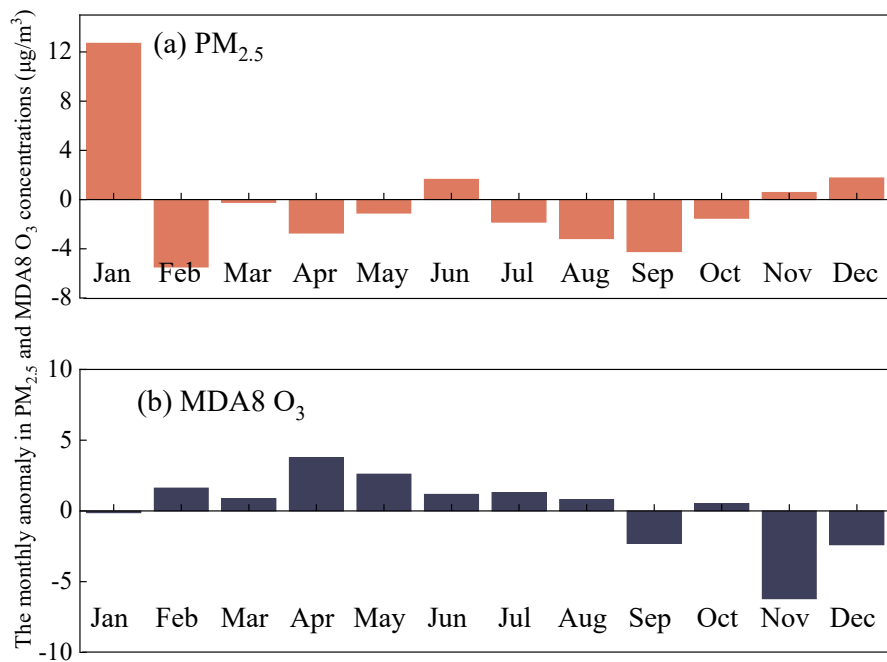


Figure 8 The monthly anomaly in $\text{PM}_{2.5}$ (a) and MDA8 O_3 concentrations (b) driven by the changing daily emissions for Jiangsu Province in 2022, based on the MLR model.

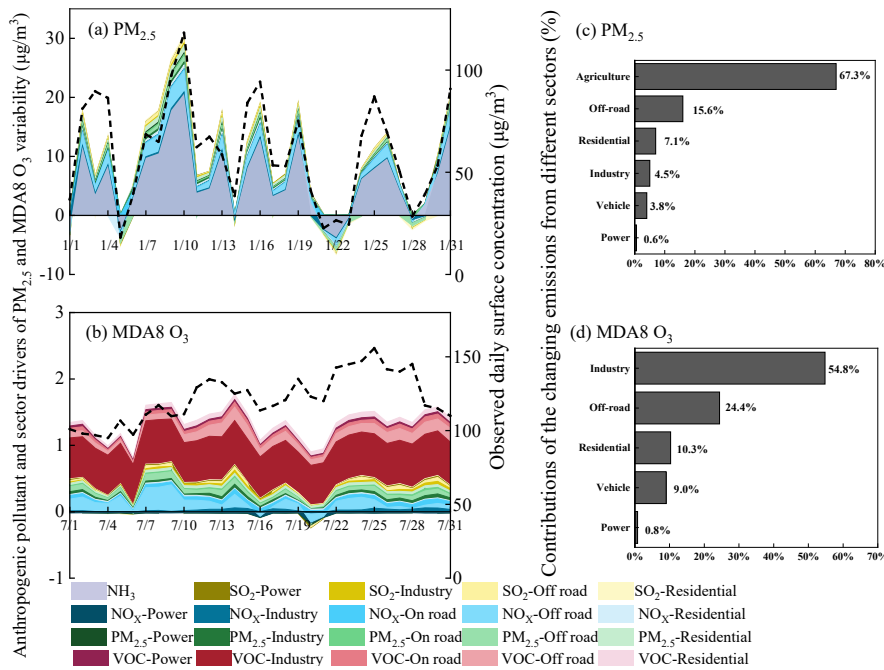


Figure 9 Anthropogenic pollutant and sector drivers of PM_{2.5} and MDA8 O₃ variability. (a) and (b) illustrate the contributions of pollutant-sector combinations to the variability of PM_{2.5} in January and that of O₃ in July, derived from SHAP analysis. The black dashed lines represent the observed daily ground-level concentrations of PM_{2.5} and MDA8 O₃. (c) and (d) provided the contributions of the changing emissions from different sectors, with those of various precursor species aggregated.